

https://dspace.org/

Designing a low cost passively Q-switched solid state laser transmitter

Madlala, Bigboy

2017

https://hdl.handle.net/10539/24990

Madlala, Bigboy (2017) Designing a low cost passively Q-switched solid state laser transmitter, University of the Witwatersrand, Johannesburg, <http://hdl.handle.net/10539/24990>

Downloaded from a DSpace repository. https://dspace.org/

Designing a low cost passively Q-switched solid state laser transmitter



by

Bigboy Madlala

A Dissertation submitted to the Faculty Of Science in partial fulfillment of the requirements for the degree of

Master of Science by Research only

in the School of Physics, University of the Witwatersrand, Johannesburg.

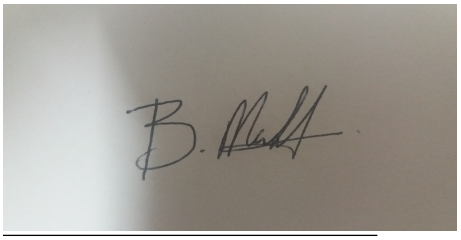
Supervisors:

Prof. Andrew Forbes
Mr. Louwrens van Schalkwyk

July 11, 2017

Declaration

I declare that this dissertation is my own, unaided work. It is being submitted for the Degree of Master of Science at the University of the Witwatersrand, Johannesburg. It has not been submitted before for any degree or examination at any other University.



(Signature of candidate)

11th day of July 2017 in Johannesburg

Abstract

A discrete Q-switched laser that gives a side-lobed single pulse as a laser output was implemented; followed by studying energy extraction efficiencies and pulse characterisation. The aim was to help design a passively Q-switched laser that gives a smooth single pulse of optimum energy as a laser output. The smoothness feature in a single pulse is important in some applications such as range finding. The concepts are demonstrated both experimentally and numerically; the latter using Fox-Li approach to modeling resonator modes with the Fresnel's integral for the system under study.

In the first two chapters, fundamentals of how a laser works and the spatial mode development are studied. In chapter 1, the principles of a laser are discussed: absorption, spontaneous and stimulated emission. Also, different types of pumping sources and resonator configurations that can be used are discussed. In chapter 2, the focus is on developing spatial modes of a laser. The fundamental and high order modes are discussed together with their propagation laws. Then a numerical method is used to find the eigenmodes of an arbitrary resonator configuration. This numerical method is used to simulate propagation of a fundamental mode and the simulation results are compared to analytical propagation laws. Then, this numerical method is used to simulate a laser resonator. The eigenmode of the lowest loss in the resonator was found.

In chapters 3 and 4, experimental work is done on a Q-switched laser where the focus is on the overall laser performance. In chapter 3, Q-switched laser output energies are studied for different combinations of Q-switch transmission values and output coupler reflectivities. In addition, the influence of spatial modes on a Q-switched pulse shape and pulse width are studied, taking into account beam divergence. In chapter 4, conclusions and future work are presented. In future work, the knowledge of spatial mode influence on pulse shape, pulse width and beam divergence from chapter 3 is exploited. Then particular resonator configuration that gives optimised output results (Q-switched laser output energy, beam divergence, pulse shape and pulse width) is chosen. On that particular resonator, different Q-switch transmission values are studied, but now looking only at beam divergence and pulse width. Also, some suggestions on further improving laser performance are given.

Acknowledgments

My supervisor, Prof. Andrew Forbes. I would like to thank you for giving me the opportunity to work with you; expose me to different ways of learning and instilling principles of getting the work done. Most importantly, I thank you for imparting the laser Physics knowledge to me and academic guidance from my Honours level to Masters. The time I spent working with you was immensely great, both academically and socially, I wholeheartedly appreciate it.

Airbus Defence and Space Optronics and its staff. Thank you for the financial support that made my MSc possible and for providing me with the environment to work in; especially the beautiful laser laboratories.

Johan Steyl, thank you for all the knowledge you shared with me regarding lasers, in particular, Q-switched lasers. Working alongside you, I have subliminally learned to understand lasers from the basic principles as you always emphasized.

Louwrens van Schalkwyk, thank you for guiding me throughout my MSc journey.

Aggie Mdluli, I would like to thank you for the career advice and instilling determination in me. I admire your everyday learning attitude.

Structured light laboratory group, it was great working with you guys, I really enjoyed, especially listening to your talks that are mind stimulating on each and every project each of you were working on. It was a privilege working with you.

Friends: Masego Erens, Itumeleng Mokgosi, Neo Mashego, Petition Nkoana, thank you for always encouraging and supporting me throughout my academic career. I honestly appreciate your time and effort you put during great and difficult times.

My parents, thank you for always being there for me. Most importantly, I would like to thank you for raising me to be the best person I am today. I promise to not disappoint you and will keep on being a good person. I am indebted to you for the time, effort you put to raise me.

My siblings, thank you for being there with me especially during hard times. Your happiness is contagious, it helped a lot during school stress.

Contents

1 Introduction **1**
- 1.1 Historical background and literature review . . . 1
  - 1.1.1 Background to the study . . . 1
  - 1.1.2 Focus of the study . . . 2
  - 1.1.3 Data used in study . . . 3
  - 1.1.4 Contribution of the study . . . 3
- 1.2 Fundamentals of lasers . . . 4
  - 1.2.1 Basic principles . . . 4
  - 1.2.2 Gain . . . 8
  - 1.2.3 Resonator . . . 9
  - 1.2.4 Q-switching . . . 14
- 1.3 Outlook of dissertation . . . 18
- 1.4 Summary . . . 18

2 Laser resonator **19**
- 2.1 Wave nature analysis of laser beams . . . 19
  - 2.1.1 Approximate solution of the wave equation . . . 19
  - 2.1.2 Fundamental and higher order modes . . . 21
- 2.2 Analytical propagation of laser beams . . . 24
  - 2.2.1 Fundamental mode propagation laws . . . 24
- 2.3 Numerical approaches . . . 28
  - 2.3.1 The Fresnel integral . . . 28
  - 2.3.2 The Fox-Li method . . . 31
  - 2.3.3 The Matrix method . . . 32
- 2.4 Simulation results . . . 33
  - 2.4.1 Comparison of numerical and analytical propagation of Gaussian beams 33
  - 2.4.2 Multiple round trip of stable cavity with aperture (known Gaussian beam) . . . 36
  - 2.4.3 Higher order mode . . . 41
- 2.5 Summary . . . 41

3 Experimental setup and results **43**
- 3.1 Flashlamp pumped solid-state laser assembly . . . 43
  - 3.1.1 Construction overview . . . 43
  - 3.1.2 Laser assembly components . . . 44

3.1.3 Complete laser assembly 50
3.2 Output performance 52
3.2.1 Output energy 52
3.2.2 Spatial mode results 58
3.2.3 Q-switched temporal mode results 60
3.3 Summary 60

4 Conclusions and Future work **62**
4.1 Conclusions 62
4.2 Future work 63
4.2.1 General modal analysis (time and space) 63
4.2.2 Improvements to laser design 64

List of Figures

1.1 Schematic showing fundamental principles of a laser in a 2-level energy system. Atom (red circle) excitation by a photon (sinusoidal wave) from the ground state (level 1) to the excited state (Level 2) during absorption process (diagram (a)). Decay of the atom back to the ground state and emission of a photon by spontaneous emission process (diagram (b)). Stimulation of the atom from the excited state back to the ground state by a photon and thus emit another photon by stimulated emission process (diagram (c)). 5

1.2 Schematic showing atom transitions in a 3-level energy system. Atom excitation from ground state (level 1) to the high excited state (level 3). Followed by radiationless decay of the atom to the low excited state (level 2). Lastly, transition of the atom back to the ground state and emit a photon. 7

1.3 Schematic showing atom transitions in a 4-level energy system. Atom excitation from ground state (level 1) to the high excited state (level 4). Followed by radiationless decay of the atom to the low excited state (level 3). Then atom transition to the lower excited state(level2) and emit a photon. Lastly, radiationless decay of the atom back to the ground state. 8

1.4 A schematic diagram of a passive resonator with a Gaussian mode. M_1 and M_2 are the curved mirrors of radius of curvature R_1 and R_2, respectively. w_0 is the beam radius (marked by red dashed line) of the Gaussian mode (blue solid line). Z_1 and Z_2 are the distances from the beam waist of mirror M_1 and M_2, respectively. 9

1.5 A diagram showing plots of g-parameters. Common resonator configuration indicated (red plot). Stable resonator region (blue shaded) and symmetrical resonator configuration (red dashed line) (as drawn by F. Dominec et al (November 2007)). 10

1.6 Paraxial ray propagating through a linear optic. 12

1.7 Schematic showing atom transitions between a 4-level energy active medium and 4-level saturable absorber. Laser radiation from the active medium excites atoms in the saturable absorber from the ground state (sa1) to the excited state sa2 by absorption process. Followed by transitioning of the atom from the excited state sa2 to the lower excited state sa3. Then excitation of the atom from the lower excited state sa3 to the higher excited state sa4 by absorption process. Iteratively, transition of the atom from the higher excited state sa4 back to the lower excited state sa3. 15

1.8 Schematic of temporal evolution of gain, resonator losses and a passively Q-switched laser pulse. Solid line (blue) showing how gain stored in the 4-level energy system active medium is linearly growing during pumping until threshold condition is reached (point (a)). Solid line (green) showing how resonator losses (Q-switch, mirror, diffraction and/or scattering losses) change. solid line (red) showing building up of the passively Q-switched laser starting at (i), reaching maximum at (ii) and end at (iii). Point (a), (b) and (c) indicates initial population inversion, population at second threshold point and final population, respectively. 16

2.1 Schematic showing a paraxial field amplitude and wavefront variation during beam propagation. 20
2.2 Schematic showing a gaussian profile (blue solid line) and its image. 21
2.3 An image showing Hermite-Gaussian modes. 23
2.4 The image showing Laguerre-Gaussian modes (As coded by Ziofil (November 2012)). 24
2.5 Schematic showing how the amplitude and wavefront of the Gaussian mode change with propagation. w_0 is the beam waist and the wavefront is flat (radius of curvature of the wavefront is at infinity) at that point ($z = 0$). θ is the half beam divergence. 27
2.6 Superposition of spherical waves at point P from propagation of electric field distribution given on plane F. 29
2.7 Simulation plots of Gaussian beam propagation compared to theory (Eq.(2.37)). Simulation plots (red circle markers) of Gaussian beam of 1064 nm wavelength and 110 μm initial beam radius propagating through free space and this compared to theory (blue solid line). 34
2.8 Simulation plots of Gaussian beam propagation compared to theory (Eq.(2.40)). Simulation plots (red asterisk markers) of Gaussian beam of 1064 nm wavelength and radius of curvature at infinity initially propagating through free space and this compared to theory (blue solid line). 35
2.9 Schematic of a stable cavity with an aperture along with its lens guide. Diagram (A) shows a stable cavity of a plane mirror (R_1) and curved mirror (R_2) with aperture. This shows how beam properties (W_0 is the minimum beam waist and wavefront) of a steady-state mode change with propagation distance (z). Diagram (B) is a lens guide representation of the resonator in diagram (A) with a curved mirror being replaced by two lenses. 36
2.10 Simulation results showing evolution of a steady-state mode for a stable cavity with an aperture . The intensity distributions (blue solid line) after a particular number of round trips (titled on each image) are plotted against the normalised radius (dividing the mirror axis (X) throughout by the radius value(2 mm)). 37
2.11 Simulation results showing relative amplitudes of modes with increasing number of round trips. 39

2.12 Simulation results of a stable cavity with an aperture. Steady-state mode which is Gaussian (black circles) of 211 μm beam size (calculated at $1/e^2$ of maximum intensity) at R_2 mirror is obtained for an aperture size of 320 μm. The plots are fitted with a Gaussian function (green solid line) 40
2.13 Simulation results of a stable cavity with a loss line. Steady-state mode which is TEM_{10} at R_2 mirror is obtained for a loss line at the central axis ($x = 0$) of the mirror. The plots (black circles) are fitted with Hermite-Gaussian function for TEM_{10} mode (green solid line) which is given by Eq.(2.18). 41

3.1 Schematic diagram of a passively Q-switched solid-state laser. The electric circuit is used to power the pump source which then excites the gain medium. The Q-switch generates short pulses in the nanosecond regime after saturation, then laser light leaves through partially reflective mirror (R_2). 44
3.2 A photograph of two coated mirrors (R_2 and R_1) of unknown optical and geometrical properties. 45
3.3 The measured transmission of optical wavelength spectra through mirror R_1 (green solid line) and R_2 (red dotted line). The diamond markers for 1064 nm wavelength. 45
3.4 The interference pattern and structure of mirrors R_1 and R_2 surface. A and B are interference patterns with corresponding mirror structure indicated by blue traces of mirror R_1 and R_2, respectively. 46
3.5 A photograph of Nd:YAG crystal used in constructing the laser. 47
3.6 A schematic of the LC circuit used to power Xenon flashlamp. The capacitance (C) of C= 20μF was used for the circuit. An in-house developed test transmitter (power supply) unit was used to drive the LC circuit. 48
3.7 An oscilloscope trace of the current pulse applied to the Xenon flashlamp. . . 49
3.8 A photograph of Xenon flash lamp (transparent) and one side of pump cavity (white in colour). 49
3.9 A photograph of an assembled Nd:YAG laser setup. The geometrical length of cavity (length between two mirrors) of 80 mm 50
3.10 A Photograph of the experimental setup to generate a Q-switched pulse from a laser and capture transverse mode patterns at the far field with their corresponding generated pulse and output energy. The laser light coming from a laser is split by the beam splitter which is orientated at an angle where 99 % of the reflected light is directed to the energy detector connected to the energy meter. The pulse detector is connected to the oscilloscope alongside the beam splitter. The remaining 1 % of the laser light gets transmitted to a flat mirror, then reflected to the collimator of 1542 mm focal length for far field projection. The reflected light from the collimator is then captured by the CCD beam profiler which connected to the computer and placed at the focal length of the collimator. 51
3.11 Experimental plots of an Nd:YAG laser in long-pulsed operation and solid line of best fit. 52

3.12 Experimental plots of an Nd:YAG laser in long-pulsed operation for different reflectivity output couplers and their respective solid lines of best fit. Plots for the reflectivity of 40, 47 and 70 % indicated by green stars, blue circles, and red squares markers, respectively. Together with their lines of best fit of corresponding colours to their markers. 53
3.13 Experimental plots of a Q-switched Nd:YAG laser using different Q-switch transmission values and step dashed lines were drawn to fit the plots. Q-switch transmission values of 40, 53 and 65 % were used and their plots are indicated by purple circles, red circles, and green square markers, respectively. 55
3.14 Experimental plots of a Q-switched Nd:YAG laser using different Q-switch transmission values per mirror reflectivity and step lines drawn to fit the plots. Q-switch transmission values of 40, 53 and 65 % were used and these are indicated by green squares, red circles and purple circles, respectively. Mirror reflectivity of 40, 47 and 70 % indicated by solid line, dashed line and dotted line, respectively. 56

4.1 Experimental plots of a Q-switched Nd:YAG laser for a setup with and without a Samarium flow tube for different Q-switch transmission values, and step lines fitted to the plots. Dashed lines and solid lines presenting a setup with and without a Samarium flow tube, respectively. Q-switch transmission values of 40, 53 and 65 % indicated by green squares, red circles and purple circles markers, respectively. 65

List of Tables

1.1 Ray transfer matrix of common optical systems 13

3.1 Optical properties of the Nd:YAG gain medium and Cr^{4+}:YAG Q-switch for σ_{gs} and σ_{es} mentioned in Eq.(1.18). 47
3.2 Comparison of experimental and theoretical output energy using different Q-switch transmission values (Cr^{4+}:YAG properties given in Table (3.1)) per mirror reflectivity. 57
3.3 Comparison of experimental and theoretical output energy using different Q-switch transmission values (guessed properties) per mirror reflectivity. 57
3.4 Captured far field Nd:YAG laser spatial mode pattern with varying aperture size and corresponding full beam divergence. 58
3.5 Captured far field Q-switched Nd:YAG laser spatial mode pattern with varying aperture size and corresponding full beam divergence. 59
3.6 Detected Q-switched pulse with varying aperture size fitted with Gaussian profile and the corresponding pulse width. 60

4.1 Captured far field Q-switched spatial mode pattern with corresponding pulse generated and measured full beam divergence and pulse width for different Q-switch transmission values. 64

Chapter 1

Introduction

1.1 Historical background and literature review

1.1.1 Background to the study

A laser is a device that emits coherent light after a process of optical amplification which takes place inside a cavity [1],[2]. Lasers are different from other light sources since they can emit light that is directional (spatial coherence) and monochromatic (temporal coherence), and thus high radiance can be directed to a specific point. It is these features of a laser that play a major role in material cutting, welding, shaping and for use as pointers. The laser light monochromaticity feature is used extensively in measurement such as in interferometry and high-resolution spectroscopy. Other interesting applications of lasers are optical disk drives, laser printers, and barcode scanners, fiber-optics and construction; where they are used as a leveling device.

In the year 1917, Albert Einstein described the theory of stimulated emission, which is the primary principle of a laser [3],[4]. At first, a MASER (Microwave Amplification by Stimulated Emission of Radiation) was built by C. Townes in 1954 which led to an idea of a laser in the year 1958 by C. Townes and A. Schawlow [5]. The idea could not be tested because they did not know what suitable gain medium to use until the first actual demonstration of a laser by T. Maiman in the year 1960 at Hughes Research Laboratories where he used a pink ruby crystal as a gain medium [6]. This laser was flashlamp pumped and gave out red light of 694 nm wavelength. From advancement of a ruby laser, other states of gain medium such as gas and liquid were researched. In the year 1961, the helium-neon (He-Ne) gas laser was demonstrated and this was the first laser to give a continuous light as a laser output [7]. This first laser operated in the infrared regime of the spectrum at a wavelength of 1.15 μm. In the year 1962, it was modified to operate at a visible regime of 632.8 nm wavelength, as a result, being the first laser to give a continuous laser output in visible spectrum [7].

The ruby laser gave a pulse of irregular spikes as the laser output [8]. The inspiration of wanting to concentrate these irregular spikes into a single pulse led to the discovery of Q-switching by R.W. Hellwarth in 1961. Q-switching is a technique used to generate short

pulses i.e. in the nanosecond regime, by modulating intracavity losses [8]. Initially, saturable absorbers used for Q-switching were based upon organic dyes which were later replaced by F_2^-:LiF colour center crystal since organic dyes were more degradable due to their light sensitivity property. Consequently, they needed replacement from time to time. In addition, plastic materials' low thermal limitation such as low melting point restricted the applications of passive Q-switches. Currently Cr^{4+}:YAG crystal is considered to be an ideal saturable absorber, especially for the Nd-doped gain medium that gives high peak power [9]. This is because Cr^{4+} ions provide a high absorption cross section of the laser wavelength, and YAG crystal provides the required mechanical, chemical and thermal properties required for long life [10].

The advent of a Q-switched laser opened doors to new applications, such as range finding, which is particularly used in the military [8],[11]. In range finding, a pulse is sent to the target and then gets reflected back. By knowledge of the entire flight time, to and from the target, and the speed of light, the range of how far the target is from the laser can be calculated. Depending on peak power, i.e pulse energy, and pulse width and beam divergence, a particular range can be measured. For long ranges, high peak power, and small beam divergence is required [12]. Small beam divergence enables precise selection of one target.

1.1.2 Focus of the study

In obtaining an ideal pulse for application in range finding, a smooth pulse of high peak power is required [12]. Achieving high peak power means a pulse of high energy and narrow pulse width (since power is a ratio of energy to pulse width), to obtain high energy, a large volume of the gain medium should be utilised. This comes at a cost since it results in getting a pulse(s) with side lobes and broader pulse width [13], which reduces peak power. In order to get rid of the side lobes and obtain short pulses, an aperture is inserted inside a laser [2]. This reduces laser output energy significantly, and consequently, reduces peak power. So in optimizing laser efficiency, this relationship of laser energy with pulse width should be kept in mind. Here, we use a different approach to get rid of the side lobes while not compromising laser output energy. We try out different resonator configurations to get short pulses and use different combinations of Q-switch transmission values and mirror reflectivities to get high output energies.

Also, eigenmodes of an arbitrary laser resonator are studied and this is done computationally. There are two methods usually used to simulate solid state laser resonators, namely, the Gaussian method approach and the Fox-Li method [14]. The former cannot predict mode superposition and competition. The latter is the first method that was used for simulating laser modes, i.e. solutions to the wave equation, which took into account diffraction effects and it was implemented by A.G. Fox and T. Li at the Bell Telephone Laboratories in the early 1960s [15]. Fox-Li method is a numerical method based on iteratively applying Collin's integral between two mirrors, and thus, finding the lowest loss mode [15][16]. This method was first used to calculate modes in a laser resonator which then was proposed to be a Fabry-Perot interferometer [15].The Fox-Li method was further improved by incorporating the matrix method, and this reduced computation time significantly [17]. The matrix

method exploits the constancy in the transformation function throughout the field propagation to and from the mirrors for a symmetric resonator [17]. Here, we use the improved version of the Fox-Li method to simulate the spatial modes of a laser which is passive. A passive resonator is a resonator composed of only two mirrors and nothing between them (free propagation), which is usually a finite diameter planar or finite diameter curved end mirrors. For advanced resonators, such as ones having optical elements in the resonator, an ABCD matrix in Collin's integral can be used. Also, a more general Collin's integral even for misaligned optical elements which takes into account the tilt in the phase term of electromagnetic waves is at our disposal[18].

1.1.3 Data used in study

When optimizing a Q-switched laser, several strategies such as pulse width minimization and pulse energy maximization can be used, depending on the required laser performance and/or laser specifications [19]. In general, extraction efficiency strategy is the preferred way to optimize a Q-switched laser [19]. Also, it should be noted that there is a unique combination of output coupler reflectivity and Q-switch transmission that optimizes a passively Q-switched laser for a particular initial population inversion [19].

1.1.4 Contribution of the study

Generating a very short pulse which is comparable to a shorter excited state relaxation time of a gain medium results in intrinsically having two pulses as a laser output [20]. This is because after the first pulse, the gain gets restored since there is still a population of atoms in the upper state, which then results in secondary pulsing [20]. Alternatively, this secondary pulsing may be attributed to the presence of saturation when the initial transmission of output coupler was low enough [20]. In range finding when optimizing a Q-switched laser, only a single pulse is adequate to measure range. Therefore, a minimum size of pulse width so as to have only a single pulse should be taken into account. This is beneficial because operating in a single pulse minimizes detection from an enemy. Generating a short energetic pulse enables long ranges to be measured and allows a precise selection of the target. Since here we look at the spatial modes and temporal modes, the analysis of both would help in obtaining a short energetic pulse for range finding application.

1.2 Fundamentals of lasers

1.2.1 Basic principles

Photon absorption and spontaneous emission

There are three processes responsible for atomic transitions between energy levels, namely, photon absorption, spontaneous and stimulated photon emission [21]. A simplified non-degenerate 2-level system of energy difference $E_2 - E_1$, where E_2 and E_1 are the energies of an excited state and ground state respectively, shall be used to demonstrate the concepts.

In thermal equilibrium, the ground state is more occupied compared to the excited state(s) [22]. In photon absorption, an incident photon on a ground state atom is required to excite it to the excited state (Fig(1.1)). Since the molecules, atoms and ions have a set of specific energy levels, a photon has to have a specific energy to excite the ground state atom [6]. That energy is given by

$$E = h\nu, \tag{1.1}$$

where $E = E_2 - E_1$, h is Planck's constant and ν is the frequency of the incident photon.

In spontaneous photon emission, no photon is required to initiate the process, an electron that is already in the excited state has a finite probability to decay back to the ground state (Fig.(1.1)) since $E_2 > E_1$. As a result, a photon that has energy E gets emitted and can propagate in any direction. The decay process depends on the lifetime of the electron in that excited state.

The finite probabilities mentioned above depend on the population in the energy levels which are described by atomic rate equations [21]. Letting N_1 be the population of electrons per unit volume at time t at ground state and N_2 the population at the excited state. Therefore, for non-degenerate energy levels, $N_{total} = N_1 + N_2$. In an absorption process, when an external signal of frequency ν passes between energy levels, the rate of population depletion from the ground state is proportional to population in the ground state and the radiation energy density, and it is given by [21]:

$$\frac{\partial N_1}{\partial t} = -B_{12}\rho\left(\upsilon\right)N_1, \tag{1.2}$$

where B_{12} is the Einstein's coefficient for stimulated absorption with units cm^3/s^2J, and ρ is the energy density per unit frequency of the incoming photons. The partial derivatives are used since also ambient conditions, such as changing in background temperatures can influence population change between energy levels.

In a spontaneous emission process, a rate of population depletion from an excited state is proportional to that population, and thus

$$\frac{\partial N_2}{\partial t} = -A_{21}N_1, \tag{1.3}$$

where A_{21} is the coefficient of spontaneous emission with units s^{-1}.

Since the decay process depends on the lifetime of the electron in that excited state. A solution to Eq.(1.3) is

$$N_2(t) = N_2(0)\, e^{-\frac{t}{\tau_{21}}}, \tag{1.4}$$

where $\tau_{21}\left(= {A_{21}}^{-1}\right)$ is the lifetime for the spontaneous emission process to occur.

Stimulated Emission

In stimulated emission, an external signal (photon) stimulates an atom that is in an excited state [3],[23]. That stimulated atom has a finite probability to transition to the ground state. As an atom goes to the ground state, it emits a photon that has the same phase as the incident photon and the two photons propagate in the same direction as shown in Fig.(1.1)

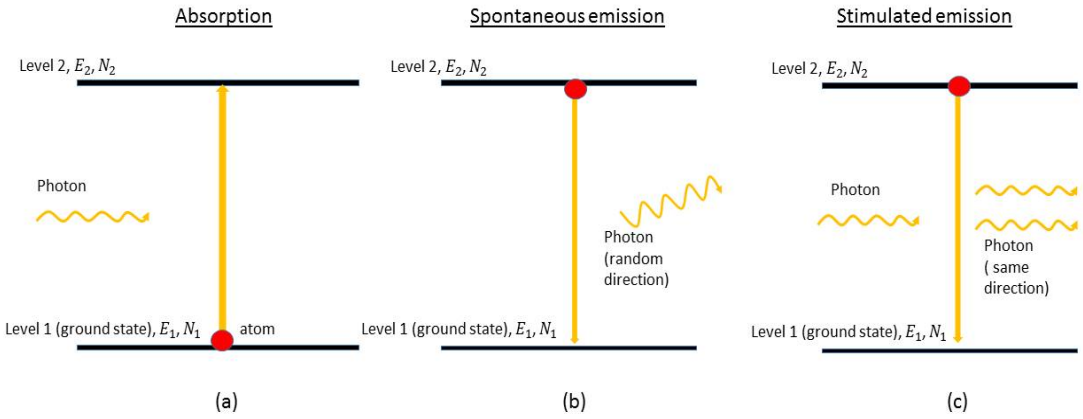


Figure 1.1: Schematic showing fundamental principles of a laser in a 2-level energy system [23]. Atom (red circle) excitation by a photon (sinusoidal wave) from the ground state (level 1) to the excited state (Level 2) during absorption process (diagram (a)). Decay of the atom back to the ground state and emission of a photon by spontaneous emission process (diagram (b)). Stimulation of the atom from the excited state back to the ground state by a photon and thus emit another photon by stimulated emission process (diagram (c)).

It is this type of coherent radiation that comes out of a laser. The rate of population depletion from an excited state is proportional to the population of the excited state and the radiation energy density, and it is given by

$$\frac{\partial N_2}{\partial t} = -B_{21}\rho\left(\upsilon\right)N_2, \tag{1.5}$$

where B_{21} is the Einstein coefficient for stimulated emission with units cm^3/s^2J, and ρ is the energy density per unit frequency of the incoming photons.

Population inversion

In thermal equilibrium, the ground state is more populated than the excited state(s), which makes it impossible to achieve stimulated emission since the external photon passing between the energy levels would be absorbed. In having a situation where the stimulated emission process occurs, more than half the population of atoms should be in an excited state(s) compared to the population in the ground state. In order to achieve this, an external supply of energy is required. This energy source is commonly known as a pump source, and the condition of having more population of atoms in the excited state(s) than in the ground state is called a population inversion. In order to sustain a population inversion, a specific structure of energy levels is required, and thus, a 2-level energy system is not a good system to use since it cannot sustain a population inversion [7]. Hence, 3-level and 4-level energy systems are good systems to use.

In a 3-level system, initially at thermal equilibrium, the level 1 (ground) state is more populated than the level 2 and 3 (excited) states. Energy would have to be pumped into the system to excite more than half of the atoms to transition to higher energy state, which in this case is level 3. This level is known as the pump band which in turn comprises of bands in such a way that an excitation process occurs over a broad spectral range. From level 3, atoms transition by fast radiationless decay to level 2 (metastable state), causing level 2 to be more populated than level 3 and 1. As a result, population inversion is achieved. Furthermore, atoms transition from level 2 to 1 by the slow spontaneous emission process and release a photon of frequency known to be a laser transition frequency. The entire processes of a 3-level system are shown in Fig.(1.2)

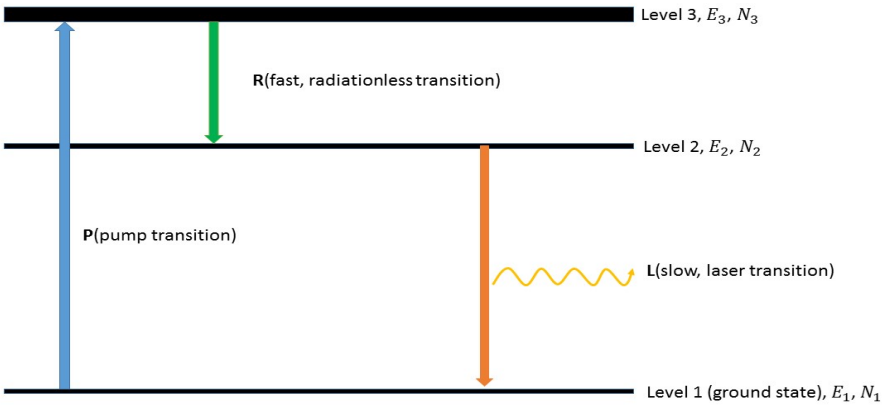


Figure 1.2: Schematic showing atom transitions in a 3-level energy system. Atom excitation from ground state (level 1) to the high excited state (level 3) [21]. Followed by radiationless decay of the atom to the low excited state (level 2). Lastly, transition of the atom back to the ground state and emit a photon.

In a 4-level system, a similar process occurs. Energy is pumped into a system which is in thermal equilibrium, and more than half of the atoms transition from level 1 to 4. Then atoms transition by a fast radiationless decay to level 3 (metastable state), causing level 3 to be more populated than 4 and 1. Thus, population inversion is achieved. Furthermore, atoms transition from level 3 to 2 by the slow spontaneous emission process, and as a result, release a photon of laser transition frequency. Lastly, atoms transition from level 2 to 1 by a fast radiationless decay. The entire process is shown in Fig.(1.3)

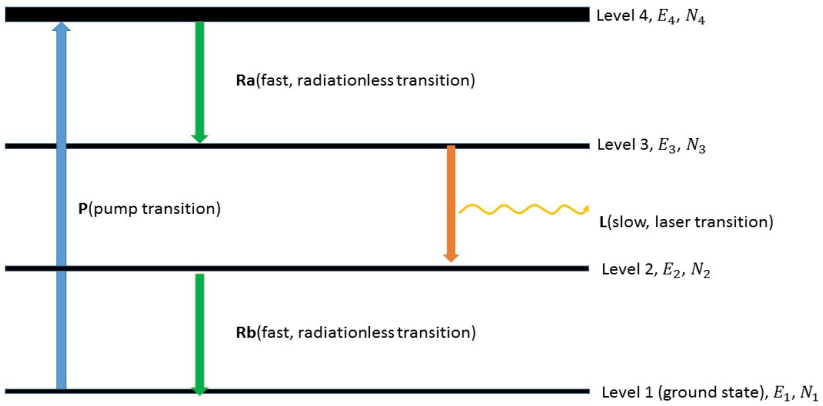


Figure 1.3: Schematic showing atom transitions in a 4-level energy system [21]. Atom excitation from ground state (level 1) to the high excited state (level 4). Followed by radiationless decay of the atom to the low excited state (level 3). Then atom transition to the lower excited state(level2) and emit a photon. Lastly, radiationless decay of the atom back to the ground state.

Comparing a 4-level system with a 3-level system, it can be seen from the above figures that less energy is required for transition from level 3 to 2 for a 4-level system than for transition from level 2 to 1 for a 3-level system. As a result, lower lasing threshold energy is required for a 4-level system than for a 3-level system [21].

1.2.2 Gain

The above-mentioned fundamentals of a laser occur in a structure called a gain or active medium. The gain medium can be in various forms, namely, gas, liquid, and solid. In a gas medium, a gas is contained in a glass tube, and the excitation of atoms is caused by a collision of electrons and/or atoms inside [2]. The first laser that was built of such gain medium was the Helium-Neon (He-Ne) laser [7].

In a liquid gain medium, a solvent is mixed with a chemical substance, for example, an organic dye like sodium fluorescein which would form a solution. Then molecules are excited to a state of being ready to emit stimulated radiation. Also, semiconductors (separate class from solid state) such as GaAs (gallium arsenide) can be used as a gain medium in which electrons from the valence band get excited to the conduction band. A solid-state gain medium is used in this project because of strong mechanical and thermal strength. In a solid-state medium, a solid crystal such as Nd:YAG or Ruby is used. In thermal equilibrium there is more population in ground state than excited states; as a result, to achieve population inversion, the gain medium has to be disturbed. This is done by applying external energy to the gain medium. There are various means this external energy can be applied; such as, electrical, optical, chemical etc. The mentioned fundamentals of a laser enable light

amplification when these proccesses occur inside a containment, which is called a resonator.

1.2.3 Resonator

In a laser, the necessary structure for light oscillation is known as an optical resonator; which is usually referred to as just a resonator. A resonator is comprised of two faced mirrors (M_1 and M_2) with or without a gain medium between and the latter is usually referred to as a passive resonator (shown in Fig.(1.4)) and the former an active resonator [13]. One of the mirrors is fully reflective whilst the other is partially reflective at a given wavelength. The laser light exits through the partially reflective mirror. There are various configurations of a resonator and this depends on the curvature of the mirrors (R_1 and R_2) and resonator length (L) used [24]. For simplicity, a passive resonator would be used to explain resonator mode parameters. The Gaussian mode, which would be explained in great detail in the next chapter, is used since it is a fundamental mode and other higher modes scale from it [8].

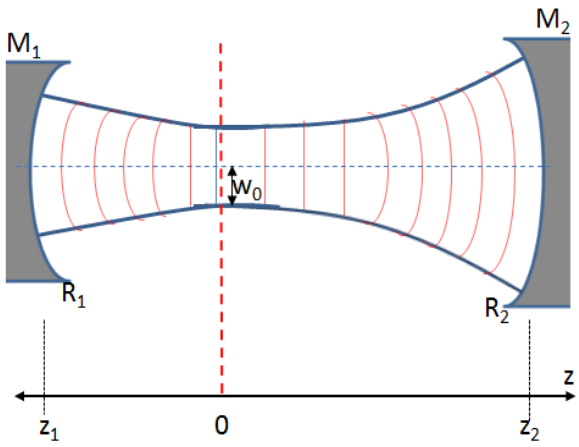


Figure 1.4: A schematic diagram of a passive resonator with a Gaussian mode [25]. M_1 and M_2 are the curved mirrors of radius of curvature R_1 and R_2, respectively. w_0 is the beam radius (marked by red dashed line) of the Gaussian mode (blue solid line). Z_1 and Z_2 are the distances from the beam waist of mirror M_1 and M_2, respectively.

The beam radii of a Gaussian mode at mirror M_1 and M_2 are related to resonator mirror geometry and resonator length by

$$w_1^4 = \left(\frac{\lambda R_1}{\pi}\right)^2 \frac{R_2 - L}{R_1 - L}\left(\frac{L}{R_1 + R_2 - L}\right), \tag{1.6}$$

and

$$w_2^4 = \left(\frac{\lambda R_2}{\pi}\right)^2 \frac{R_1 - L}{R_2 - L}\left(\frac{L}{R_1 + R_2 - L}\right), \tag{1.7}$$

where w_1 and w_2 are the beam radii at mirror M_1 and M_2, respectively, and λ is the laser wavelength [8].

The beam waist which can be in or outside the resonator is given by

$$w_0^4 = \left(\frac{\lambda}{\pi}\right)^2 \frac{L\left(R_1 - L\right)\left(R_2 - L\right)\left(R_1 + R_2 - L\right)}{\left(R_1 + R_2 - 2L\right)^2}. \tag{1.8}$$

These are the general equations governing Gaussian mode properties and resonator configuration. The following are the g-parameters relating mirror curvature and resonator length:

$$g_1 = 1 - \frac{L}{R_1}, \tag{1.9}$$

and

$$g_2 = 1 - \frac{L}{R_2}, \tag{1.10}$$

for mirror M_1 and M_2 respectively. These parameters differ for different resonator configuration, as it will be shown in the next chapter. The g-parameters are usually represented diagrammatically for better visualisation.

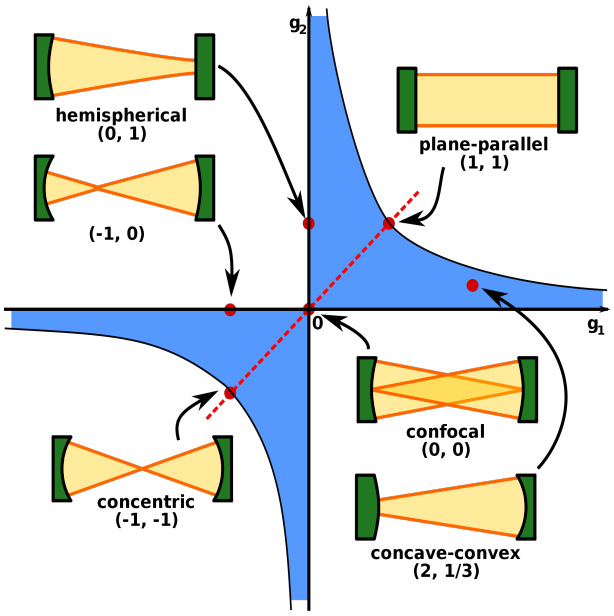


Figure 1.5: A diagram showing plots of g-parameters. Common resonator configuration indicated (red plot). Stable resonator region (blue shaded) and symmetrical resonator configuration (red dashed line) (as drawn by F. Dominec et al (November 2007)).

In Fig.(1.5) a stable region is the region where

$$0 < g_1 \times g_2 < 1, \tag{1.11}$$

otherwise the resonator is unstable [13]. In a stable resonator, the light radiation is confined between the mirrors. The opposite is true for the unstable resonator. This would further be explained by use of ray transfer matrix later on. Beam parameters of all resonators

shown in Fig.(1.5) can be calculated using Eq.(1.6) and Eq.(1.7). For example, for a plano-concave resonator, beam waist at mirror M_1 ($R_1 = \infty$) and M_2 ($R_2 > L$)

$$w_1^4 = \left(\frac{\lambda R_1}{\pi}\right)^2 \left(\frac{R_2 - L}{R_1\left(1 - \frac{L}{R_1}\right)}\right) \left(\frac{L}{R_1\left(1 + \frac{R_2}{R_1} - \frac{L}{R_1}\right)}\right), \tag{1.12}$$

Therefore simplifies to

$$w_1^2 = \left(\frac{\lambda}{\pi}\right) \left[L\left(R_2 - L\right)\right]^{1/2}, \tag{1.13}$$

for mirror M_2

$$w_2^4 = \left(\frac{\lambda R_2}{\pi}\right)^2 \left(\frac{R_1\left(1 - \frac{L}{R_1}\right)}{R_2 - L}\right) \left(\frac{L}{R_1}\right), \tag{1.14}$$

therefore simplifies to

$$w_2^2 = \left(\frac{\lambda}{\pi}\right) R_2 \left(\frac{L}{R_2 - L}\right)^{1/2}. \tag{1.15}$$

In a real laser, a resonator comprises of a gain medium, lens etc. between the mirrors. Therefore, effects caused by these optics such as the lens should be taken into account when analysing laser modes. This is done by using the ABCD matrix law, also known as a ray transfer matrix.

In a ray transfer matrix, the type of rays that are used to study stability and/or losses of resonators are paraxial rays [24]. These types of rays have a small angle ($\cos(x') \approx 1$), where x' is the angle between the ray and axial axis (a line perpendicular to parallel mirrors). The propagation of paraxial rays are studied in linear optics such as lens etc. An example of paraxial ray propagating through an optic is shown in Fig.(1.6).

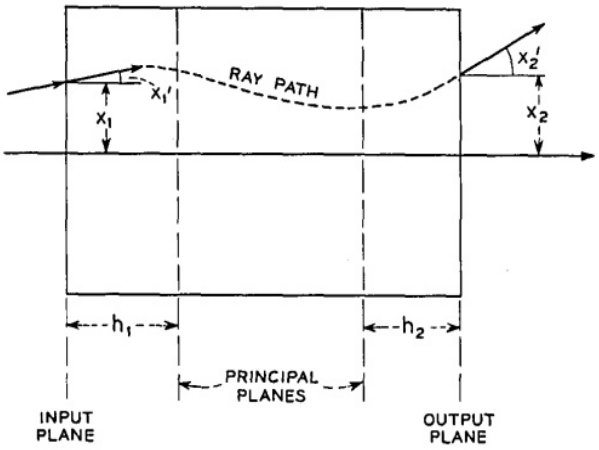


Figure 1.6: Paraxial ray propagating through a linear optic [24].

In Fig.(1.6), x_1 and x_2 are distances from the axial axis before and after propagation of paraxial ray respectively, of which $x_1^{'}$ and $x_2^{'}$ are angles from the axial axis before and after propagation of paraxial ray respectively. Relating the initial and final properties of a paraxial ray after passing through the optic

$$\begin{pmatrix} x_2 \\ x_2^{'} \end{pmatrix} = \begin{bmatrix} A & B \\ C & D \end{bmatrix} \begin{pmatrix} x_1 \\ x_1^{'} \end{pmatrix}, \tag{1.16}$$

where the square matrix is what is referred to as a ray transfer matrix and also called the ABCD matrix law. This matrix is an optical transformation of paraxial rays through an optic and it is an optical property of an optic. A few ray matrices for common optics are listed in Table (1.1).

Table 1.1: Ray transfer matrix of common optical systems

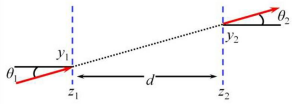
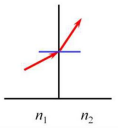
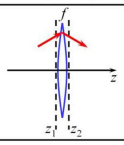
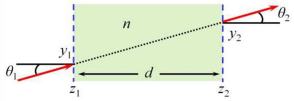
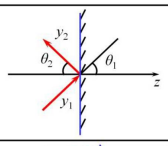
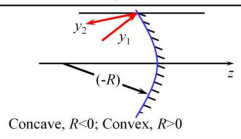
No.	Optical System	Ray-Transfer Matrix
1		$\begin{vmatrix} 1 & d \\ 0 & 1 \end{vmatrix}$
2		$\begin{vmatrix} 1 & 0 \\ 0 & n_1/n_2 \end{vmatrix}$
3		$\begin{vmatrix} 1 & 0 \\ -1/f & 1 \end{vmatrix}$
4		$\begin{vmatrix} 1 & d/n \\ 0 & 1 \end{vmatrix}$
5		$\begin{vmatrix} 1 & 0 \\ 0 & 1 \end{vmatrix}$
6	 Concave, $R<0$; Convex, $R>0$	$\begin{vmatrix} 1 & 0 \\ 2/R & 1 \end{vmatrix}$

Table (1.1) represents common optical systems encounter by a ray along with their ray transfer matrix [21]. The optical system no. 1 represents two planes, z_1 and z_2; with free space between them that are separated by distance d. Optical system no. 2 is a plane where a ray experiences a change of refractive index from n_1 to n_2. Optical system no. 3 represents a thin lens of focal length f. The optical system no. 4 is a medium of thickness d and refractive index n. Optical systems no. 5 and 6 represent flat and curved reflective planes of radius of curvature at infinity and R, respectively. In an active resonator, the effects caused by these optical systems needs to be taken into account.

1.2.4 Q-switching

A simple active resonator only comprises of a gain medium, two mirrors and an input pump source. It can be made even more complicated than this by inserting other optical systems such as a Q-switch to generate short pulses. The Q in a Q-switch stands for a quality factor, which is basically described by a ratio of energy stored to energy losses (shown in Eq.(1.17)). In a laser, the energy is stored in a gain medium and energy losses are mainly produced by the mirrors and the Q-switch. A Q-switched pulse is a laser pulse of high peak power in nanosecond regime, and is essentially generated by modulating intra-cavity losses. Two techniques can be used to generate these types of pulses; active and passive Q-switching [8].

In active Q-switching, an active control element such as electro-optic and acousto-optic modulators are used. Electro-optic modulator requires an external trigger that applies external field to the crystal, and as an effect, introduces birefringence in the crystal. On the other hand, acousto-optic modulator makes use of ultrasound wave to modulate losses in the resonator. In passive Q-switching, which is the technique under study, a saturable absorber is used, and since this does not require external triggering, a compact, low cost and simple laser design is achievable [8],[9],[26]. Furthermore, a passive Q-switch is efficient in spatial and longitudinal modes selection [27].

$$Q = \frac{2\pi E_{stored}}{E_d}, \tag{1.17}$$

where E_{stored} is the energy stored in the gain medium and E_d represent energy losses in the resonator.

In generating a Q-switched pulse, intra-cavity losses are modulated and as a consequence, the quality factor of the laser is modulated. A Q-switch initially blocks laser radiation from oscillating in the resonator i.e. low quality factor (high energy losses and low stored energy). During this period, laser radiation is absorbed by the Q-switch which then results in exciting atoms in the Q-switch from the ground state to the excited state (as shown in Fig.(1.7)). Since the quality factor is low, more gain is stored i.e. stored energy, in the gain medium to overcome the energy losses, thus, improving the quality factor (low energy losses and high stored energy). Ultimately, the Q-switch saturates, this leads to a rapid build-up of a laser action due to the higher gain in the rod compared to the same resonator but with no Q-switch (long-pulsed operation).

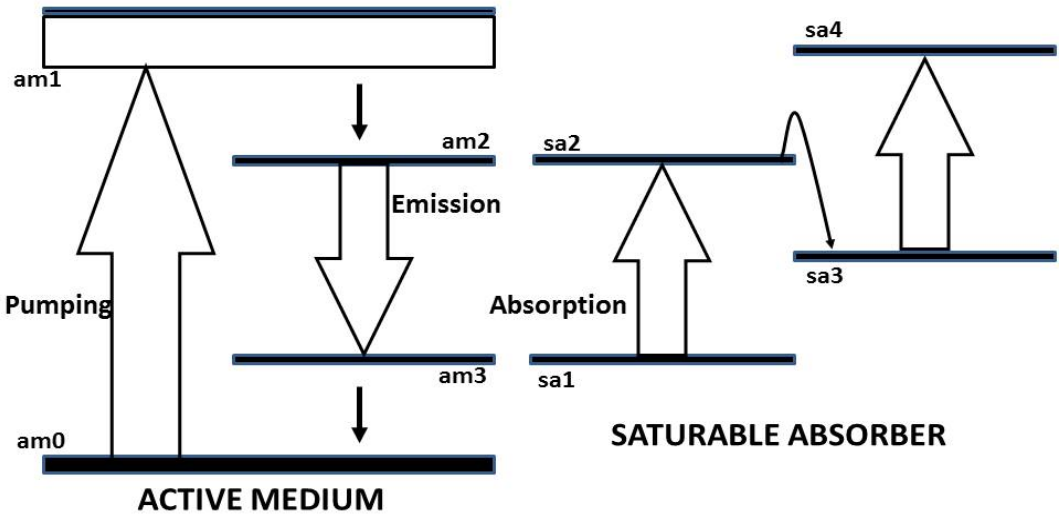


Figure 1.7: Schematic showing atom transitions between a 4-level energy active medium and 4-level saturable absorber [11]. Laser radiation from the active medium excites atoms in the saturable absorber from the ground state (sa1) to the excited state sa2 by absorption process. Followed by transitioning of the atom from the excited state sa2 to the lower excited state sa3. Then excitation of the atom from the lower excited state sa3 to the higher excited state sa4 by absorption process. Iteratively, transition of the atom from the higher excited state sa4 back to the lower excited state sa3.

In Fig.(1.7), the Q-switch (saturable absorber) absorbs laser radiation from the gain medium. For the 4-level energy system Q-switch, the ground state sa1 population gets excited to the excited state sa2. Then atoms transition by a fast radiationless decay to level sa3. At this point, population inversion is achieved in the Q-switch since more population is at level sa3 than level sa2 and sa1. Then the Q-switch starts to saturate allowing laser radiation oscillations (seen by building up of a laser pulse shown in Fig.(1.8)). However, during laser radiation oscillations, there is still some additional losses due to excited state absorption occurring between level sa3 and sa4. Transitions between level sa3 and sa4 do not saturate because of fast relaxation of sa4 level [28],[8],[29].

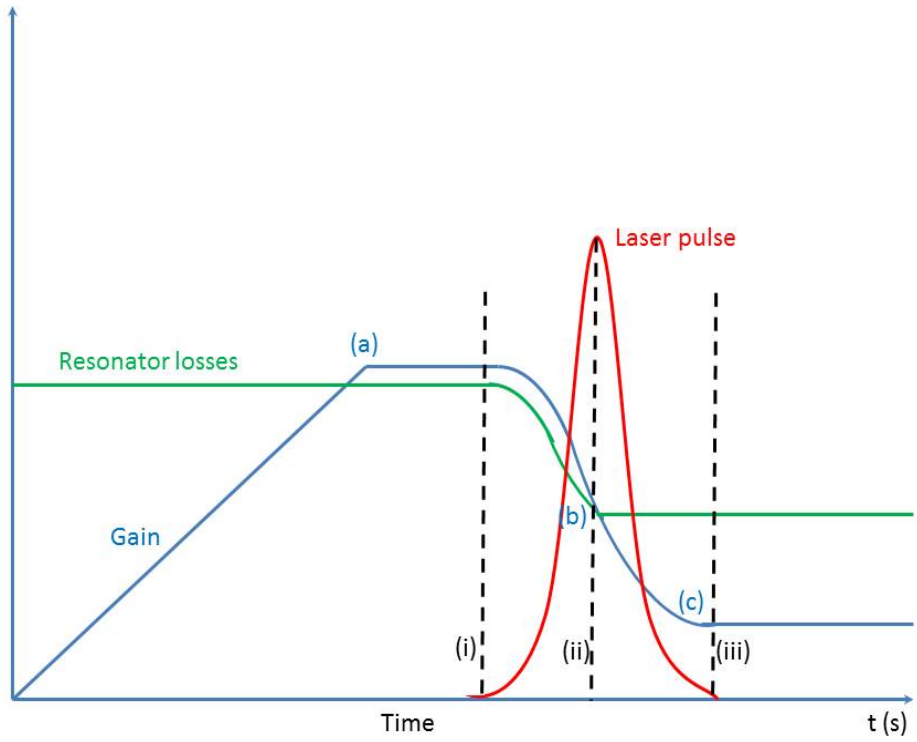


Figure 1.8: Schematic of temporal evolution of gain, resonator losses and a passively Q-switched laser pulse [8]. Solid line (blue) showing how gain stored in the 4-level energy system active medium is linearly growing during pumping until threshold condition is reached (point (a)). Solid line (green) showing how resonator losses (Q-switch, mirror, diffraction and/or scattering losses) change. solid line (red) showing building up of the passively Q-switched laser starting at (i), reaching maximum at (ii) and end at (iii). Point (a), (b) and (c) indicates initial population inversion, population at second threshold point and final population, respectively.

A passive Q-switch has an initial T_0 and maximum T_{max}(bleached) transmissions. From initial to maximum transmission, higher photon densities should be applied. The maximum transmission does not necessarily reach 100% because of unsaturable excited state absorption of a Q-switch. This maximum transmission is calculated according to

$$T_{max} = \exp\left(\delta \times \ln\left(T_0\right)\right), \tag{1.18}$$

where $\delta = \frac{\sigma_{es}}{\sigma_{gs}}$ with σ_{gs} and σ_{es} being the absorption cross section of the ground and excited state of the Q-switch, respectively [8].

As more laser radiation is applied to a Q-switch, after reaching its maximum transmission, a Q-switch bleaches, and thus, allows laser oscillation [30]. The Q-switching is rapid (faster than long-pulsed operation), which then results in shorter laser output pulse(s).

At lasing threshold, initial population inversion n_i of a passively Q-switched operation which is obtained from the coupled rate equations is given by

$$n_i = \frac{\ln\left(\frac{1}{T_0^2}\right) + \ln\left(\frac{1}{R}\right) + L}{2\sigma l}, \tag{1.19}$$

where R and L are the mirror reflection and round trip resonator losses (due to diffraction or scattering of laser radiation with optics), respectively [31],[32],[10].

The population from the metastable state (am2 in Fig.(1.7)) then gets reduced as it transitions to lower laser levels during laser pulse formation. When the pulse reaches a maximum, the population left at metastable state is then given by

$$n_t = \frac{1}{2\sigma l} \times \left(\ln\left(\frac{1}{R}\right) + L + \delta \ln\left(\frac{1}{T_0^2}\right)\right), \tag{1.20}$$

where σ and l are the stimulated cross section and geometrical length of the active medium, respectively.

In calculating energy of a laser pulse generated, final population inversion n_f left after laser pulse is required, and that can be found from n_i and n_f relationship

$$n_i - n_f = n_t \times \ln\left(\frac{n_i}{n_f}\right) + \frac{(1-\delta)\ln\left(1/T_0^2\right)}{2\sigma l \alpha}\left[1 - \left(\frac{n_f}{n_i}\right)^{\alpha}\right], \tag{1.21}$$

where $\alpha = \frac{\sigma_{gs}}{\gamma\sigma}$ and γ is the degeneracy factor ($\gamma = 2$ or 1 for 3-level or 4-level energy system of the active medium).

Using numerical methods, n_f can be calculated. Then one can calculate the theoretical output energy

$$E_{out} = \frac{h\nu A}{2\sigma\gamma} \ln\left(\frac{1}{R}\right) \ln\left(\frac{n_i}{n_f}\right), \tag{1.22}$$

where A is a cross sectional area of the active medium. Also, energy stored in the gain medium can be calculated from

$$E_{stored} = \frac{Alh\nu n_i}{\gamma} \tag{1.23}$$

1.3 Outlook of dissertation

Here, a low cost passively Q-switched solid-state laser which is used in range finding is designed. Considering this application, a smooth single high peak power pulse is required for long ranges i.e high output energy and short laser pulse. The smoothness feature of the laser pulse is critical in enabling single target detection. Since high energy is required as a laser output, spatial modes for different resonator configurations of a laser will be studied because of direct proportionality between the two. Also, numerical methods will be used to simulate the spatial modes of laser resonators.

1.4 Summary

In this chapter, the primary focus was on laser principles and resonator configurations. In consequence, achieving those principles required discussion on various pumping sources and gain media. Any one of the available pumping sources and gain media can be chosen depending on the performance requirements of a laser. Likewise, a particular resonator configuration can be chosen depending on the required laser performance, as an example, a plano-concave resonator was chosen to mathematically show how Gaussian beam parameters change with resonator parameters.

Chapter 2

Laser resonator

The focus here is to develop spatial modes of a laser. Firstly, fundamental and high order modes are discussed together with their propagation laws. Then a numerical method is used to find the eigenmodes of an arbitrary resonator configuration. This numerical method is then used to simulate propagation of a fundamental mode and the simulation results are compared to analytical propagation laws. Then, this numerical method is used to simulate a laser resonator. The eigenmode of the lowest loss in the resonator is found.

2.1 Wave nature analysis of laser beams

2.1.1 Approximate solution of the wave equation

In the previous chapter, only the laser mode parameters such as beam size was studied inside a resonator cavity. This only takes into consideration the geometrical properties of optics in dictating laser mode parameters. However, in practical lasers, apertures that are used are finite and thus, have to take into account diffraction effects when analysing laser modes. This is done by looking at the wave nature of light . As a result, the time independent scalar wave equation is used [24]. This is given as

$$\nabla^2 E + k^2 E = 0, \tag{2.1}$$

where E is the electric field and $k = \frac{2\pi}{\lambda}$ is the propagation constant in the medium.

The laser beams behave like plane waves but with nonuniform field distribution, for instance, light traveling in z direction, the field is given by

$$E = \psi(x, y, z)e^{-ikz}, \tag{2.2}$$

Where $\psi(x, y, z)$ is a slowly varying complex function describing transverse properties of light with propagation distance z.

Substituting E into Eq.(2.1) gives

$$\frac{\partial^2\psi}{\partial x^2} + \frac{\partial^2\psi}{\partial y^2} + \frac{\partial^2\psi}{\partial z^2} - 2ik\frac{\partial\psi}{\partial z} = 0, \tag{2.3}$$

Applying the paraxial approximation

$$\left|\frac{\partial^2\psi}{\partial z^2}\right| \ll 2k\left|\frac{\partial\psi}{\partial z}\right| \tag{2.4}$$

and noting that

$$\left|\frac{\partial^2\psi}{\partial z^2}\right| \ll \left|\frac{\partial^2\psi}{\partial x^2}\right|, \left|\frac{\partial^2\psi}{\partial y^2}\right| \tag{2.5}$$

Eq.(2.4) and Eq.(2.5) means that the variation of propagation is slow on the scale of a wavelength and transverse scale, respectively. This is shown in Fig.(2.1)

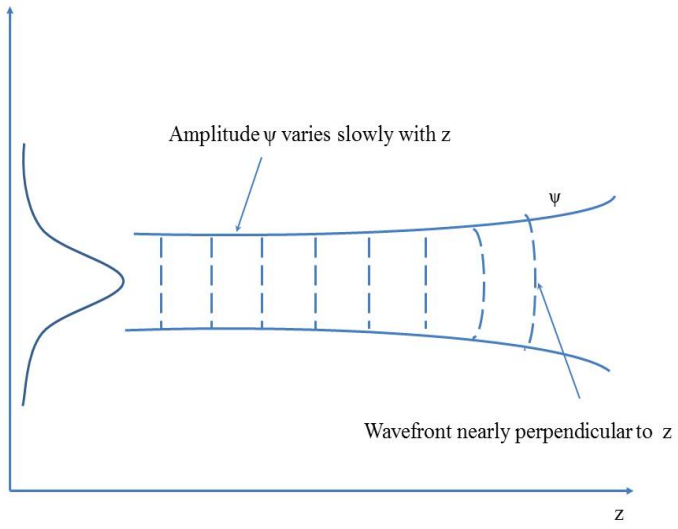


Figure 2.1: Schematic showing a paraxial field amplitude and wavefront variation during beam propagation [2].

Invoking the paraxial approximation, therefore Eq.(2.3) becomes

$$\frac{\partial^2\psi}{\partial x^2} + \frac{\partial^2\psi}{\partial y^2} - 2ik\frac{\partial\psi}{\partial z} = 0, \tag{2.6}$$

From the paraxial approximation, which implies that $\frac{\partial\psi}{\partial z}$ is small, implying that $\frac{\partial^2\psi}{\partial z^2}$ is even smaller, and thus can be neglected. One of the solutions to wave equation (Eq.(2.6)) is given by

$$\psi = \exp\left\{-i\left(P(z) + \frac{k}{2q(z)}r^2\right)\right\}, \tag{2.7}$$

this can be verified by substituting Eq.(2.7) into Eq.(2.6) and this solution is Gaussian distribution of intensity distribution as shown in Fig.(2.2), where

$$r^2 = x^2 + y^2, \tag{2.8}$$

with $P(z)$ representing a complex phase shift and assuming $\frac{\partial P}{\partial z} = -\frac{i}{q}$, this assumption would be justified later in this section. q represents a Gaussian variation of beam intensity and curvature of spherical wavefront with propagation distance z.

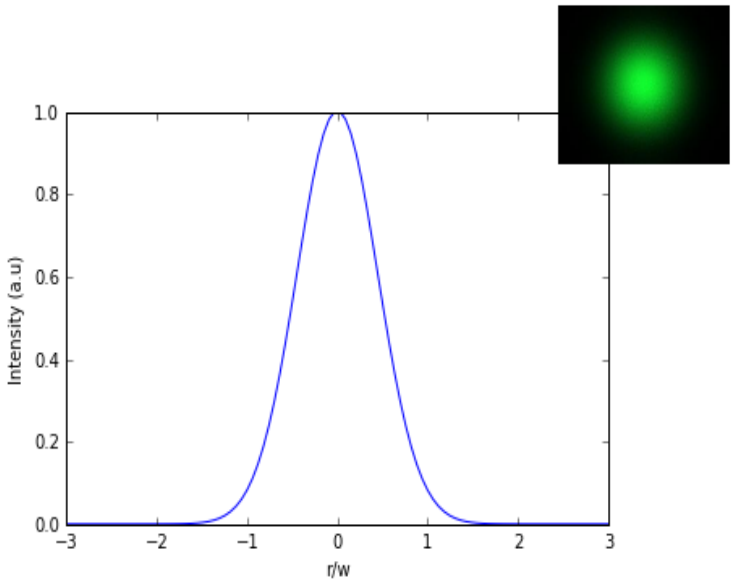


Figure 2.2: Schematic showing a gaussian profile (blue solid line) and its image [21].

2.1.2 Fundamental and higher order modes

A mode is defined as a solution to the wave equation; it was previously shown that the Gaussian beam (Eq.(2.7)) is one of the solutions. In a laser, there exists other modes such as the Hermite-Gauss, Laguerre-Gauss modes depending on the symmetry of the resonator, rectangular or circular symmetry, respectively. This is dictated by the limiting apertures used [13].

Rectangular symmetric resonator

In a Cartesian coordinate system, there exists solutions given by Hermite-Gaussian polynomials. These can be verified by substituting Hermite-Gaussian polynomials into the wave equation(Eq.(2.6)). These solutions are given by [24]

$$\psi = g\left(\frac{x}{w}\right) h\left(\frac{y}{w}\right) \exp\left\{-i\left(P + \frac{k}{2q}r^2\right)\right\}, \tag{2.9}$$

where w is a beam radius, g and h are Hermite polynomials. In order to satisfy Eq.(2.6), it is required that

$$g\left(\frac{x}{w}\right)h\left(\frac{y}{w}\right) = H_m\left(\sqrt{2}\frac{x}{w}\right)H_n\left(\sqrt{2}\frac{y}{w}\right), \tag{2.10}$$

where m and n are the number of modes in a laser beam. $H_{m/n}$ are Hermite polynomials given as: (to list a few)

$$H_0(x) = 1, \tag{2.11}$$

$$H_1(x) = x, \tag{2.12}$$

$$H_2(x) = 4x^2 - 2, \tag{2.13}$$

$$H_3(x) = 8x^3 - 12x. \tag{2.14}$$

In a laser scheme, these modes are usually represented as $\text{TEM}_{m,n}$ where TEM stands for Transverse Electro-magnetic Modes. Therefore, for TEM_{00}, we get

$$g\left(\frac{x}{w}\right)h\left(\frac{y}{w}\right) = H_0\left(\sqrt{2}\frac{x}{w}\right)H_0\left(\sqrt{2}\frac{y}{w}\right) = 1, \tag{2.15}$$

then

$$\psi = \exp\left\{-i\left(P + \frac{k}{2q}r^2\right)\right\}, \tag{2.16}$$

which is a Gaussian mode (Eq.(2.7)) and thus is represented as TEM_{00}. For TEM_{10}, we get

$$g\left(\frac{x}{w}\right)h\left(\frac{y}{w}\right) = H_0\left(\sqrt{2}\frac{x}{w}\right)H_0\left(\sqrt{2}\frac{y}{w}\right) = x, \tag{2.17}$$

then

$$\psi = x\exp\left\{-i\left(P + \frac{k}{2q}r^2\right)\right\}. \tag{2.18}$$

The laser output images are shown in Fig.(2.3).

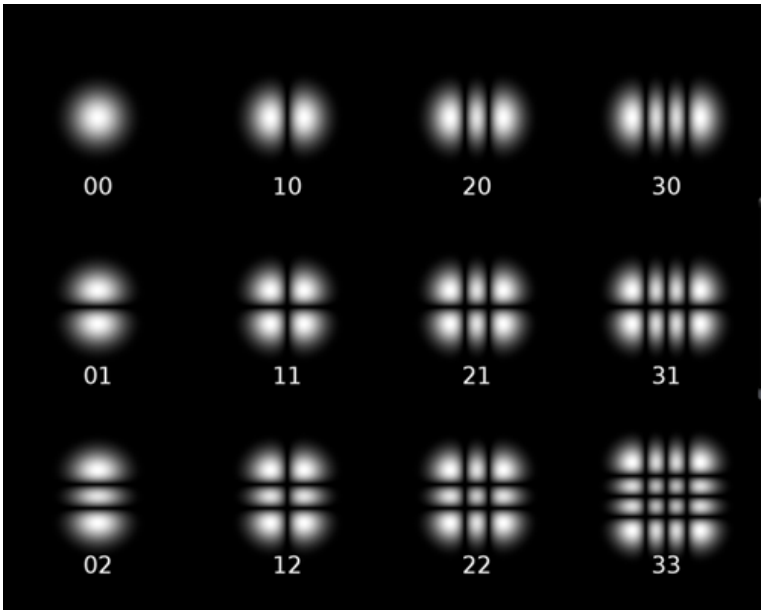


Figure 2.3: An image showing Hermite-Gaussian modes [33].

In a real laser, these types of modes can be obtained by inserting crossed metal wires inside a resonator [34].

Circular symmetric resonator

In a circular symmetric resonator, there exists Laguerre-Gaussian modes which are given by

$$\psi = g\left(\frac{r}{w}\right)\exp\left\{-i\left(P + \frac{k}{2q}r^2 + l\phi\right)\right\}, \tag{2.19}$$

with

$$g\left(\frac{r}{w}\right) = \left(\sqrt{2}\frac{r}{w}\right)^l {L_p}^l\left(2\frac{r^2}{w^2}\right). \tag{2.20}$$

Where ${L_p}^l$ is a generalized Laguerre polynomial, and p and l are the radial and angular mode numbers [24]. Some of the few Laguerre polynomials are

$${L_0}^l(x) = 1, \tag{2.21}$$

$${L_1}^l(x) = l + 1 + x, \tag{2.22}$$

$${L_2}^l(x) = \frac{1}{2}(l+1)(l+2) - (l+2)x + \frac{1}{2}x^2. \tag{2.23}$$

Similarly, these modes are represented as $\mathrm{TEM}_{l,p}$. Then a Gaussian mode is represented as $\mathrm{TEM}_{0,0}$ (as shown in Fig.(2.4)).

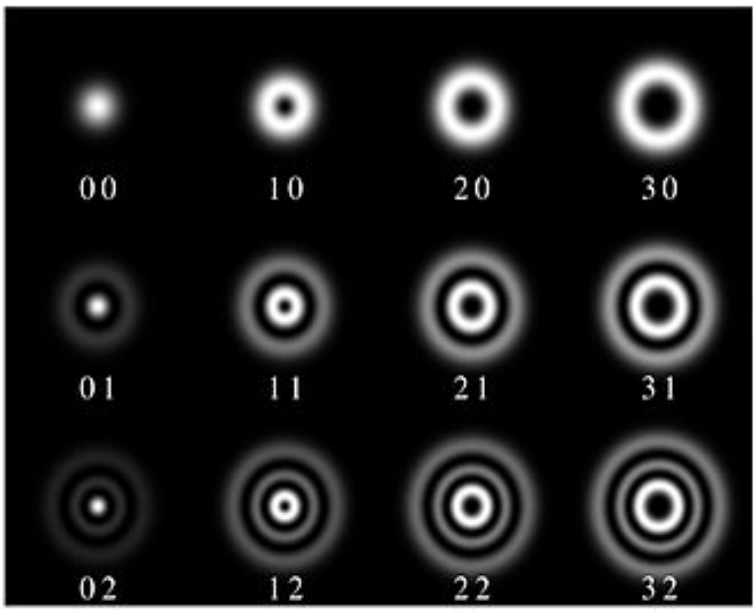


Figure 2.4: The image showing Laguerre-Gaussian modes (As coded by Ziofil (November 2012)).

2.2 Analytical propagation of laser beams

2.2.1 Fundamental mode propagation laws

As mentioned in the previous section, the fundamental mode is commonly used to explain mode properties of a laser even for high-order modes. Here propagation laws of the fundamental mode are studied extensively and extended to high-order modes propagation laws. Inserting the Gaussian solution (Eq.(2.7)) into Eq.(2.6) and then further simplifying the result by replacing $x^2 + y^2$ with r^2 gives

$$\frac{-2ik}{q}\psi - \frac{k^2r^2}{q^2}\psi - 2k\left(P\prime(z) - \frac{1}{q^2}q\prime(z)\,\frac{k}{2}r^2\right)\psi = 0, \tag{2.24}$$

then grouping like terms after dividing throughout by ψ

$$k\left(\frac{-2i}{q} - 2P\prime(z)\right) + r^2\left(\frac{1}{q^2}q\prime(z)\,k^2r^2 - \frac{k^2r^2}{q^2}\right) = 0, \tag{2.25}$$

from this, we obtain the relation

$$P\prime = -\frac{i}{q}, \tag{2.26}$$

and

$$q\prime = 1, \tag{2.27}$$

where the prime denotes differentiation with respect to z.

Integrating Eq.(2.27) gives

$$q_2 = q_1 + z, \tag{2.28}$$

where q_1 and q_2 are the input and output plane beam parameters separated by distance z, respectively.

Introducing real beam parameters related to q [24]

$$\frac{1}{q} = \frac{1}{R(z)} - i\frac{\lambda}{\pi w(z)^2}, \tag{2.29}$$

where $R(z)$ and $w(z)$ are the radius of curvature of the wavefront and beam radius with propagation distance z, respectively.

The Gaussian beam contracts to a minimum beam waist where the phase wavefront is flat. If one measures beam waist and radius of curvature of a wavefront with respect to distance z, then Eq.(2.28) becomes

$$q = q_0 + z, \tag{2.30}$$

where

$$q_0 = i\frac{\pi {w_0}^2}{\lambda}, \tag{2.31}$$

which was obtained by substituting $R \to \infty$ in Eq.(2.29) since the flatness of wavefront is similar to having a radius of curvature at infinity. w_0 denotes beam radius at the minimum beam waist.

Then substituting Eq.(2.31) into Eq.(2.30) and the results into Eq.(2.29), we obtain

$$\frac{1}{i\frac{\pi {w_0}^2}{\lambda} + z} = \frac{1}{R} - i\frac{\lambda}{\pi w^2}, \tag{2.32}$$

rationalising the denominator on the lefthand side,

$$\frac{1}{i\frac{\pi {w_0}^2}{\lambda} + z} \times \frac{z - i\frac{\pi {w_0}^2}{\lambda}}{z - i\frac{\pi {w_0}^2}{\lambda}} = \frac{1}{R} - i\frac{\lambda}{\pi w^2}, \tag{2.33}$$

which simplifies to

$$\frac{z - i\frac{\pi {w_0}^2}{\lambda}}{z^2 + \left(\frac{\pi {w_0}^2}{\lambda}\right)^2} = \frac{1}{R} - i\frac{\lambda}{\pi w^2}, \tag{2.34}$$

then equating imaginary part, we obtain

$$\frac{\frac{\pi {w_0}^2}{\lambda}}{z^2 + \left(\frac{\pi {w_0}^2}{\lambda}\right)^2} = \frac{\lambda}{\pi w^2}, \tag{2.35}$$

rearranged to

$$\frac{\pi w^2}{\lambda} = \frac{z^2 + \left(\frac{\pi {w_0}^2}{\lambda}\right)^2}{\frac{\pi {w_0}^2}{\lambda}}, \tag{2.36}$$

which then simplifies to propagation law

$$w^2(z) = {w_0}^2 \left[1 + \left(\frac{\lambda z}{\pi {w_0}^2}\right)^2\right], \tag{2.37}$$

equating the real part from equation (2.34),

$$\frac{z}{z^2 + \left(\frac{\pi {w_0}^2}{\lambda}\right)^2} = \frac{1}{R}, \tag{2.38}$$

rearranged

$$R = \frac{z^2 + \left(\frac{\pi {w_0}^2}{\lambda}\right)^2}{z}, \tag{2.39}$$

which then simplifies to propagation law

$$R(z) = z \left[1 + \left(\frac{\pi {w_0}^2}{\lambda z}\right)^2\right]. \tag{2.40}$$

Eq.(2.37) and Eq.(2.40) are important laws of Gaussian mode propagation [24],[35],[36]. They describe how Gaussian beam properties change during propagation in free space.

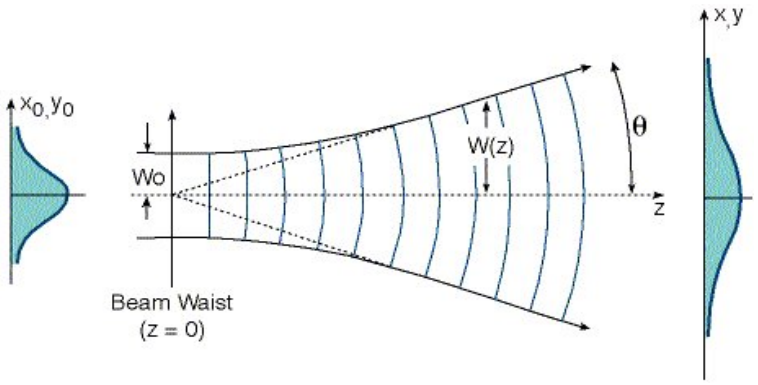


Figure 2.5: Schematic showing how the amplitude and wavefront of the Gaussian mode change with propagation. w_0 is the beam waist and the wavefront is flat (radius of curvature of the wavefront is at infinity) at that point ($z = 0$). θ is the half beam divergence.

From Eq.(2.37), when z is far from the waist, then

$$w\left(z\right) \simeq \frac{\lambda z}{\pi w_0}, \tag{2.41}$$

therefore, the half beam divergence (θ) of the fundamental mode is given by

$$\theta = \frac{\lambda}{\pi w_0}. \tag{2.42}$$

To calculate the phase shift from the minimum beam waist, substitute Eq.(2.30) into Eq.(2.26) to obtain

$$P\prime = -\frac{i}{z + i\left(\frac{\pi {w_0}^2}{\lambda}\right)}, \tag{2.43}$$

multiplying throughout by i then multiplying on the right hand side by a form of 1 $\left(\frac{-i\left(\frac{\lambda}{\pi {w_0}^2}\right)}{-i\left(\frac{\lambda}{\pi {w_0}^2}\right)}\right)$

$$iP\prime = \frac{1}{z + i\left(\frac{\pi {w_0}^2}{\lambda}\right)} \times \frac{-i\left(\frac{\lambda}{\pi {w_0}^2}\right)}{-i\left(\frac{\lambda}{\pi {w_0}^2}\right)}, \tag{2.44}$$

after simplifying

$$iP\prime = \frac{-i\left(\frac{\lambda}{\pi {w_0}^2}\right)}{1 - i\left(\frac{z\lambda}{\pi {w_0}^2}\right)}. \tag{2.45}$$

Then integrating Eq.(2.45) gives

$$iP = \ln\left(1 - i\left(\frac{z\lambda}{\pi {w_0}^2}\right)\right), \tag{2.46}$$

$$= \ln \sqrt{1 + i\left(\frac{z\lambda}{\pi {w_0}^2}\right)^2} - i \arctan\left(\frac{z\lambda}{\pi {w_0}^2}\right), \tag{2.47}$$

Therefore substituting Eq.(2.47), Eq.(2.29) and Eq.(2.7) into Eq.(2.2) and using Eq.(2.37) to simplify, we obtain

$$E(r,z) = \frac{w_0}{w} \exp\left\{-i(kz - \phi) - r^2\left(\frac{1}{w^2} + \frac{ik}{2R}\right)\right\}, \tag{2.48}$$

where

$$\phi = \arctan\left(\frac{z\lambda}{\pi {w_0}^2}\right), \tag{2.49}$$

This is the fundamental mode produced by a lot of lasers operating in single mode.

2.3 Numerical approaches

2.3.1 The Fresnel integral

Solutions mentioned in the previous sections are just approximate solutions describing field distributions that are obtained from particular laser resonators. Thus far, no exact analytical solution that describes modes obtained from laser resonators exists except for a confocal resonator [24]. However, numerical approaches such as the Fox-Li method can be used to calculate eigensolutions for arbitrary laser resonators. This method makes use of the Fresnel integral to calculate the mode with the lowest loss of a resonator. Essentially, the Fresnel integral is iteratively applied until a steady-state mode is obtained, and that would be the eigensolution to the Fresnel integral [15]. The steady-state mode is a type of mode that reproduces itself after every round trip.

The Fresnel integral is basically based on Huygen's principle. Huygen's principle states that for a given field distribution propagating from a surface into space, every point on that distribution can be considered as a source of secondary wavelets. At point P after propagating a distance r, the field is the superposition of all waves from a source, and this is clearly demonstrated in Fig.(2.6). where the starting plane is subdivided into equal intervals, few points (A, B and C) are shown.

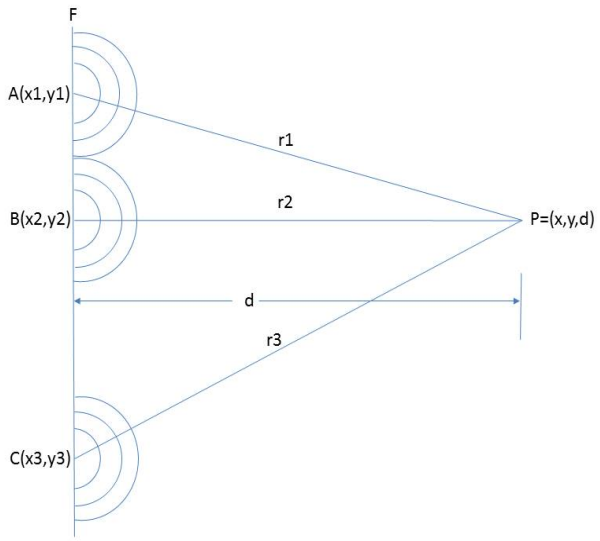


Figure 2.6: Superposition of spherical waves at point P from propagation of electric field distribution given on plane F [13].

The wave equation, Eq.(2.1), has infinite solutions and a spherical wave is one of these solutions and is given by [13]

$$E = E_0 \frac{\lambda}{r} \exp\left[i\left(wt - kr\right)\right]. \tag{2.50}$$

And thus, a spherical wave from one point of the source plane to point P is given by

$$E_i\left(P\right) = CE\left(x_i, y_i\right) \frac{\exp\left[i\left(wt - kr_i\right)\right]}{r_i} \cos\theta_i \triangle x \triangle y, \tag{2.51}$$

where r_i is the distance from (x_i, y_i), $\triangle x$ and $\triangle y$ are intervals in the x and y axis respectively. θ_i is the angle between plane F and ray r_i. C is the proportionality factor ensuring the conservation of energy.

For N number of intervals, summing over the entire source plane for a monochromatic source gives

$$E\left(P\right) = \sum_{i=1}^{N} E_i\left(P\right) = C\exp\left(iwt\right) \sum_{i=1}^{N} E\left(x_i, y_i\right) \frac{\exp\left[i\left(-kr_i\right)\right]}{r_i} \cos\theta_i \triangle x \triangle y. \tag{2.52}$$

The calculations become more accurate by increasing N. For $N \to \infty$, the summation is replaced by an integral. Applying the integral and taking into account the paraxial approximation ($\cos\theta \approx 1$) results in obtaining a surface integral known as the Kirchhoff integral, which is given by [13]

$$E\left(P\right) = \frac{i}{\lambda} \exp\left(iwt\right) \int_s E_1 \frac{\exp\left(-ikr\right)}{r} dA. \tag{2.53}$$

Usually apertures used in laser resonators are rectangular or circular in shape. For a rectangular aperture of width and height given by 2b and 2a respectively, dropping the time dependence exponential, the Kirchoff integral (Eq.(2.53)) can be written as

$$E_2(x_2,y_2)=\frac{i}{\lambda L}\int_{-b}^{b}\int_{-a}^{a}E_1(x_1,y_1)\exp\left[-ikL\sqrt{1+\left[(x_2-x_1)^2+(y_2-y_1)^2\right]/L^2}\right]dx_1dy_1, \tag{2.54}$$

where

$$r=L\sqrt{1+\left[(x_2-x_1)^2+(y_2-y_1)^2\right]/L^2}. \tag{2.55}$$

With $E_1(x_1,y_1)$ being the electric field distribution at plane 1 propagated through free space over distance L to plane 2; to give a field distribution $E_2(x_2,y_2)$. Restricting to distances much greater than the aperture size ($L >> x_1, y_1$) and assuming slow lateral changes in electric field ($x_2/L, y_2/L << 1$), r can be written as a binomial expression

$$r=L\left[1+\frac{1}{2}\left(\frac{x_2-x_1}{L}\right)^2+\frac{1}{2}\left(\frac{y_2-y_1}{L}\right)^2-\frac{1}{8}\left(\frac{x_2-x_1}{L}\right)^4-\frac{1}{8}\left(\frac{y_2-y_1}{L}\right)^4+....\right]. \tag{2.56}$$

In Eq.(2.56), some terms can be neglected depending on how far (L) from the aperture the electric field is calculated. The Fresnel number (e.g $N=\frac{a^2}{\lambda L}$) is used to determine the limit at which the approximation is applicable. In laser beams simulations, usually one of the Fresnel numbers is greater than one but less than 100 ($1<N<100$). In such cases, the Fresnel approximation is used since when $L>a,b$, fourth term in Eq.(2.56) becomes even smaller, and thus can be ignored. Then, r is approximated to be

$$r\approx L\left[1+\frac{1}{2}\left(\frac{x_2-x_1}{L}\right)^2+\frac{1}{2}\left(\frac{y_2-y_1}{L}\right)^2\right]. \tag{2.57}$$

Substituting Eq.(2.57) into Eq.(2.54), gives a Fresnel integral

$$E_2(x_2,y_2)=i\exp\left[-ikL\right]\sqrt{N_xN_y}\int_{-b}^{b}\int_{-a}^{a}E_1(x_1,y_1)\exp\left[-i\pi N_x(x_1+x_2)^2-i\pi N_y(y_1+y_2)^2\right]dx_1dy_1, \tag{2.58}$$

where $N_x=\frac{a^2}{\lambda L}$ and $N_y=\frac{b^2}{\lambda L}$ are Fresnel numbers in x and y axis, respectively. Eq.(2.58) does not have analytical solutions, the field is computed numerically.

2.3.2 The Fox-Li method

In the Fox-Li approach, the Fresnel integral (Eq.(2.58)) is iteratively applied between two mirrors facing each other until the mode of lowest loss is obtained [2] and that would be the steady-state mode. This is seen by comparing two successive fields [34]. The propagation kernel or function to be used is dependent on the geometry of the mirrors [24]. The general expression of the field transformation during propagation is given by

$$\gamma^{(1)} E^{(1)}(s_1) = \int_{s_2} K^{(2)}(s_1, s_2)\, E^{(2)}(s_2)\, dS_2, \tag{2.59}$$

$$\gamma^{(2)} E^{(2)}(s_2) = \int_{s_1} K^{(1)}(s_2, s_1)\, E^{(1)}(s_1)\, dS_1, \tag{2.60}$$

where $\gamma^{(1)}$ and/or $\gamma^{(2)}$ are eigenvalues (competition between modes) giving the phase shift and attenuation of the field per trip from one mirror to the other. $K^{(1)}$ and/or $K^{(2)}$ are the propagation kernels between the mirrors.

Generally, the propagation kernels are equal ($K^{(1)}(s_2, s_1)$=$K^{(2)}(s_1, s_2)$) but not symmetric (for example $K^{(1)}(s_2, s_1) \neq K^{(1)}(s_1, s_2)$) depending on the resonator setup [24]. For a symmetric setup, the two-dimensional integral can be written as product of one-dimensional equations, which for a rectangular symmetric system becomes

$$\gamma_x^{(1)} u^{(1)}(x_1) = \int_{-a_2}^{a_2} K(x_1, x_2)\, u^{(2)}(x_2)\, dx_2, \tag{2.61}$$

$$\gamma_x^{(2)} u^{(2)}(x_2) = \int_{-a_2}^{a_2} K(x_1, x_2)\, u^{(1)}(x_1)\, dx_1, \tag{2.62}$$

where K is given by

$$K(x_1, x_2) = \sqrt{\frac{i}{\lambda L}} \exp\left\{ -\frac{ik}{2L} \left(g_1 x_1^2 + g_2 x_2^2 - 2x_1 x_2 \right) \right\}, \tag{2.63}$$

with g_1 and g_2 being the ratios relating the mirror geometry and resonator length which are given by $g_1 = 1 - \frac{L}{R_1}$ and $g_2 = 1 - \frac{L}{R_2}$, respectively. Therefore, simulating modes, for example, of a plane-parallel resonator i.e $R_1 = R_2 = \infty$ and thus $g_1 = g_2 = 1$, of L and $2a$ resonator and mirror length, respectively, then the Fresnel integral for this particular resonator is given as

$$u^{(1)}(x_1, L) = \sqrt{\frac{i}{\lambda L}} \int_{-a_2}^{a_2} u^{(2)}(x_2) \exp\left(-\frac{i\pi}{\lambda L} \left(x_1^2 - 2x_1 x_2 + x_2^2 \right) \right) dx_2. \tag{2.64}$$

This is how the field distribution $u^{(2)}$ gets transformed into $u^{(1)}$ in free space. In general, the electric field passes through different media such as lens etc. and each different medium transforms the field differently. For the field passing through a lens for example, the field gets transformed according to [37]

$$u^{(2)} = t \times u^{(1)} \tag{2.65}$$

where

$$t = A \exp^{-\frac{ikx^2}{2f}} \tag{2.66}$$

is the transmission function in one dimension of a thin lens. $u^{(1)}$ and $u^{(2)}$ are the field immediately before and after the lens, respectively. $k = \frac{2\pi}{\lambda}$, f is the focal length of the lens and A is either equal to 1 or 0, where 1 is for the field passing through a lens and 0 otherwise.

2.3.3 The Matrix method

In general, the Fresnel integral such as the one given by Eq.(2.64) is computed over the entire mirror surface, the downside of such computation is time taken to perform this numerical calculations. In reducing computation time, the matrix method is introduced in the algorithms. This method exploits the fact that only the integrand in Eq.(2.64) changes and not the transformation function of the field during iterations. The principle of the matrix method is essentially to divide the Fresnel integral applied over the entire mirror surface into a sum of integrals applied over small mirror subdivisions [17]. To demonstrate this mathematically

$$u^{(1)}(x_1, L) = \sqrt{\frac{i}{\lambda L}} \int_{-a_2}^{a_2} u^{(2)}(x_2) \exp\left(-\frac{i\pi}{\lambda L}\left(x_1^2 - 2x_1x_2 + x_2^2\right)\right) dx_2, \tag{2.67}$$

$$= \sum_{i=0}^{M} u^{(2)}(X_2 - i\triangle x) \int_{X_2-i\triangle x}^{X_2-(i+1)\triangle x} \sqrt{\frac{i}{\lambda L}} \exp\left(-\frac{i\pi}{\lambda L}\left(x_1^2 - 2x_1x_2 + x_2^2\right)\right) dx_2, \tag{2.68}$$

where M is the total number of small divisions, $\triangle x = \frac{2X_2}{M}$ and X_2 are small subdivision and radius of the mirror, respectively.

In Eq.(2.68), it can be seen that the field is taken out of the integral. This is because for each mirror subdivision, the field is approximated to be constant. Since only the field changes during transit from one mirror to the other, expressing Eq.(2.68) in matrix form

$$\vec{u^{(1)}} = T\vec{u^{(2)}}, \tag{2.69}$$

Where $\vec{u^{(1)}}$ and $\vec{u^{(2)}}$ are the column vectors describing the field at mirror 1 and 2, respectively. T is a square matrix known as a transfer matrix. These are respectively given as

$$\vec{u^{(1)}} = \begin{pmatrix} u^{(1)}(X_1) \\ . \\ . \\ . \\ u^{(1)}(X_1 - n\triangle x) \\ . \\ . \\ . \\ u^{(1)}(-X_1) \end{pmatrix}, \tag{2.70}$$

$$T = \begin{pmatrix} T_{11} & . & . & . & T_{1M} \\ . & . & . & . & . \\ . & . & . & . & . \\ . & . & . & . & . \\ T_{M1} & . & . & . & T_{MM} \end{pmatrix}, \tag{2.71}$$

$$\vec{u^{(2)}} = \begin{pmatrix} u^{(2)}(X_2) \\ . \\ . \\ . \\ u^{(2)}(X_2 - n\triangle x) \\ . \\ . \\ . \\ u^{(2)}(-X_2) \end{pmatrix}, \tag{2.72}$$

where $T_{\mu\nu} = \int_{X_2-n\triangle x}^{X_2-(n+1)\triangle x} \sqrt{\frac{i}{\lambda L}} \exp\left(-\frac{i\pi}{\lambda L}\left(x_{1(\mu\nu)}^2 - 2x_{1(\mu\nu)}x_2 + x_2^2\right)\right) dx_2$ with $\mu, \nu = 1, 2, 3, ...M$ and $x_{1(\mu\nu)}$ is a row vector.

Incorporating the matrix method into the Fresnel integral reduces the computation time to an equivalent of a single trip computation time [17]. In studying spatial modes of a laser, Eq.(2.69) was used. Prior to that, the correctness of the transfer matrix (propagation kernel) was tested and compared to theoretical results. This was done in the following sub-section (2.4.1).

2.4 Simulation results

2.4.1 Comparison of numerical and analytical propagation of Gaussian beams

The Gaussian beam of defined initial properties (beam radius and radius of curvature) was used to test the propagation kernel given by Eq.(2.69). This was compared to theory by using fundamental propagation laws (Eq.(2.37) and Eq.(2.40)) from the previous section. The Gaussian beam in one dimension was propagated through free space, and changes in

the beam radius (shown in Fig.(2.7)) and the radius of curvature of the wavefront (shown in Fig.(2.8)) during propagation was measured.

Firstly, the mathematics was implemented into coding, then the simulations were done. In the simulation, a Gaussian beam of 110 μm beam radius, 1064 nm wavelength and flat wavefront were used as initial conditions to test the propagation kernel. As Gaussian beam propagated through free space, measurements of the beam radius and the radius of curvature were then taken at intervals of 10 mm starting from 0.

From the simulation results, measurements of the Gaussian beam parameters, beam size and radius of curvature of the wavefront were done by fitting Gaussian and quadratic functions, respectively. After the initial Gaussian beam given by $\exp\left(-\frac{x^2}{w}\right)$ has propagated by a particular distance, it should transform according to $\exp\left\{-x^2\left(\frac{1}{w^2}+\frac{ik}{2R}\right)\right\}$. In measuring the beam size, the squared of the magnitude of the complex exponential i.e $\exp\left(-\frac{2x^2}{w}\right)$ plots of the simulation results were used. The Gaussian function was then fitted to the obtained plots. From the fitted Gaussian function, the beam radius (w) was measured. In measuring the radius of curvature of the wavefront, the argument of the complex exponential i.e $-x^2\left(\frac{ik}{2R}\right)$ plots of the simulation results were used. The quadratic function was then fitted to the obtained plots. The radius of curvature of the wavefront was measured from the quadratic coefficient of the fitted quadratic function.

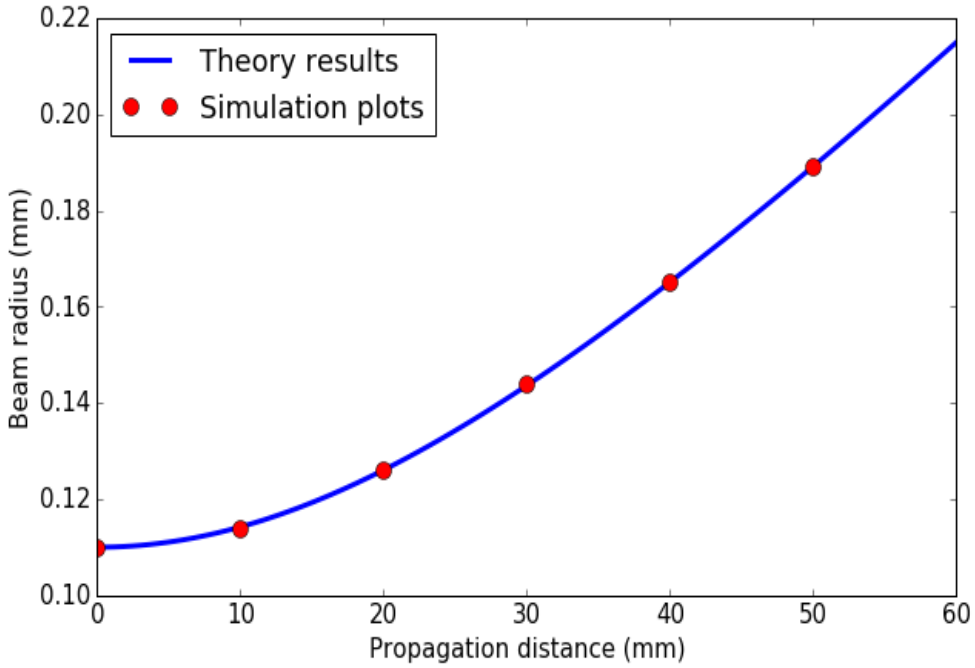


Figure 2.7: Simulation plots of Gaussian beam propagation compared to theory (Eq.(2.37)). Simulation plots (red circle markers) of Gaussian beam of 1064 nm wavelength and 110 μm initial beam radius propagating through free space and this compared to theory (blue solid line).

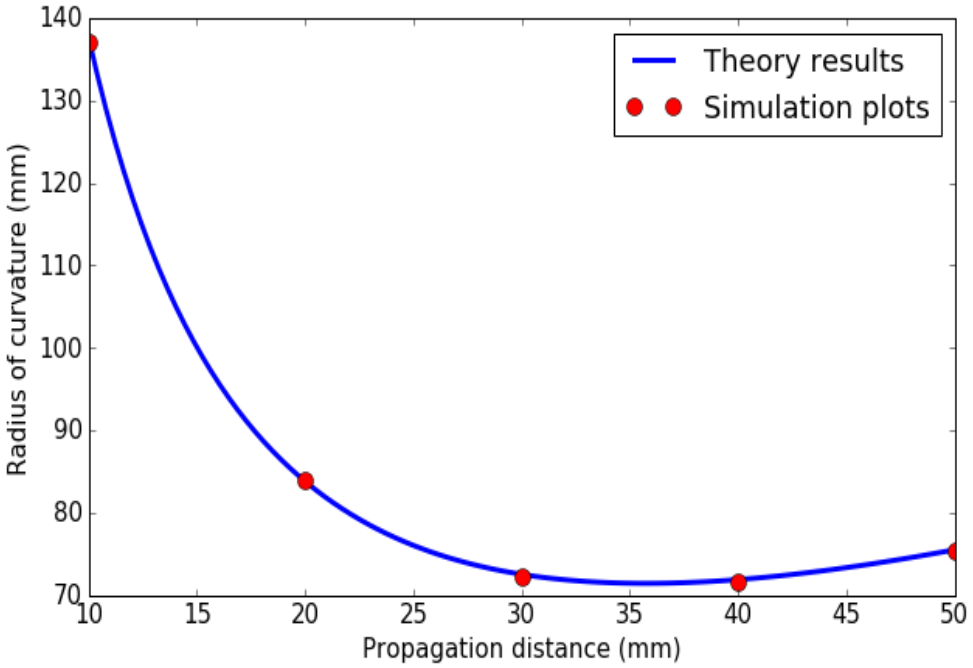


Figure 2.8: Simulation plots of Gaussian beam propagation compared to theory (Eq.(2.40)). Simulation plots (red asterisk markers) of Gaussian beam of 1064 nm wavelength and radius of curvature at infinity initially propagating through free space and this compared to theory (blue solid line).

Discussion

In Fig.(2.7) and Fig.(2.8), the simulated fundamental mode properties that are beam radius and radius of curvature of wavefront during propagation are compared to analytical theory. The simulation plots for both properties are found to be fitting correctly with the theory, and thus, proving that the propagation kernel used for the simulation is correct. For instance, in Fig.(2.7) and Fig.(2.8), all simulation plots (red circle markers) are superimposed on the blue solid line which is how the Gaussian beam radius and wavefront radius of curvature are expected to change theoretically as the Gaussian beam propagates through free space.

2.4.2 Multiple round trip of stable cavity with aperture (known Gaussian beam)

From the previous section, it was found that the propagation kernel that was used is correct. Therefore, simulation for an advanced resonator, namely, a passive resonator with an aperture and a curved mirror was studied. The idea is to obtain a steady state mode and this is studied by looking at the field distribution after a round trip. An arbitrary point is chosen within a resonator, and one round trip is completed when that arbitrary point is reached again after a field has circulated the resonator. A type of a resonator that was studied was plano-concave in which a Gaussian mode can be obtained as opposed to a plane-parallel resonator, where there exists an infinite number of modes [13]. In a plano-concave resonator, a Gaussian mode which is a fundamental mode as shown in Fig.(2.9) along with its lens guide system version is obtained by using an aperture. The aperture diameter is reduced, and thus, increasing energy losses to higher-order modes and ultimately selecting only a fundamental mode. A lens guide system is based upon periodicity, so a round trip is completed after a single period, which is from R_1 through apertures and lens to the other R_1 (Diagram (B) in Fig.(2.9)).

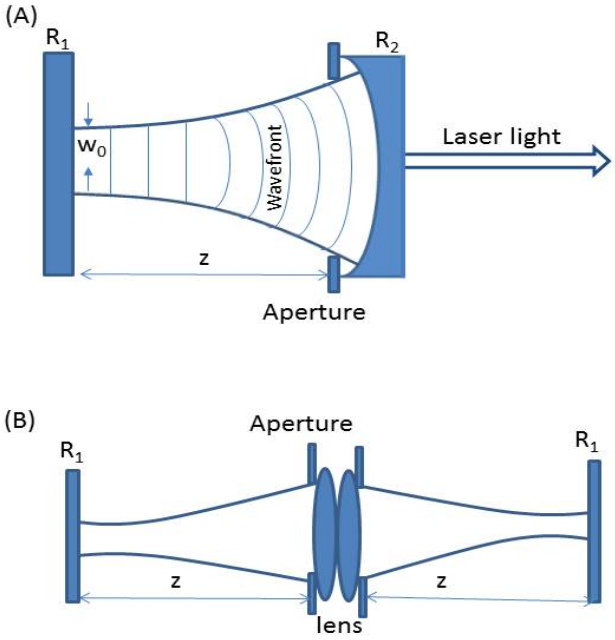


Figure 2.9: Schematic of a stable cavity with an aperture along with its lens guide. Diagram (A) shows a stable cavity of a plane mirror (R_1) and curved mirror (R_2) with aperture. This shows how beam properties (W_0 is the minimum beam waist and wavefront) of a steady-state mode change with propagation distance (z). Diagram (B) is a lens guide representation of the resonator in diagram (A) with a curved mirror being replaced by two lenses.

In the simulation, a resonator of 60 mm optical length (L) and a curved mirror of 200

mm radius of curvature with an initial uniform field $|\vec{u^{(2)}}| = 1$ for a wavelength 1064 nm (λ) was studied and the computation was still done in one dimension. These parameters were then substituted in Eq.(1.15) to roughly estimate an aperture size of 320 μm radius. Using a lens guide system as a proxy for a plano-concave resonator [38], the forward Fresnel integral (Eq.(2.69)) was applied to the field from one mirror through free space to the aperture, then through the lens using equation (2.65), and the same procedure was repeated iteratively. The advantage of using a lens guide as a proxy is that only the forward Fresnel integral is sufficient to simulate the laser output without any use of the backward integral. The mirror of 2 mm radius ($X_{1,2} = 2$ mm) was divided into 600 subdivisions($M = 600$). Then the computation was performed and the results of steady-state mode evolution for this particular resonator were plotted as shown in Fig.(2.10), where only particular intensity (obtained by squaring the field) distributions are shown after a certain number of round trips.

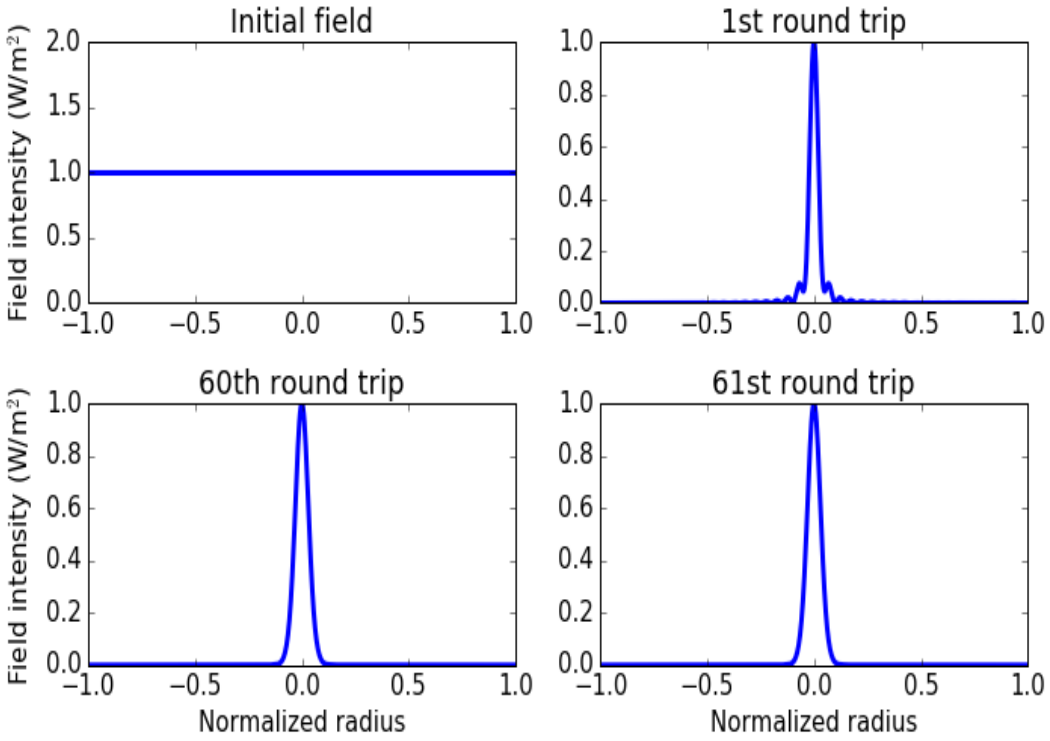


Figure 2.10: Simulation results showing evolution of a steady-state mode for a stable cavity with an aperture . The intensity distributions (blue solid line) after a particular number of round trips (titled on each image) are plotted against the normalised radius (dividing the mirror axis (X) throughout by the radius value(2 mm)).

In Fig.(2.10), looking at the distribution after 1 round trip, it can be seen from the side lobes that the field is multimode, meaning that the field has not reached the steady state for this particular resonator since the field is not Gaussian. On the other hand, after some more round trips, in this case, 60 and 61 round trips, comparing the two results, by visual inspection it is evident that there is no difference between the two intensity distributions. In order to investigate quantitatively by when the field has reached the steady state, two

successive field distributions as mentioned earlier needed to be compared. In doing this, an arbitrary point was chosen to be at the center. The results were then plotted (Fig.(2.11)).

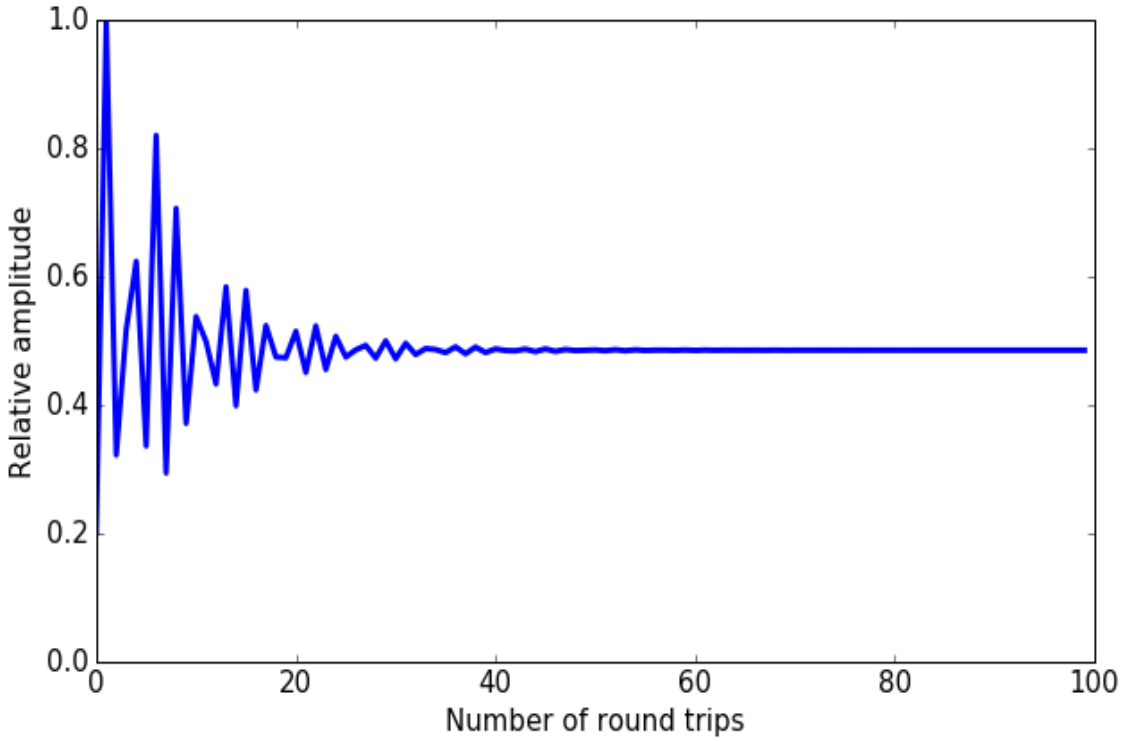


Figure 2.11: Simulation results showing relative amplitudes of modes with increasing number of round trips.

In Fig.(2.11), as the number of round trips were increased, the fluctuation of modes amplitude was found to decay to a constant. Between 0 and 30 round trips, it can be seen from the oscillation of relative amplitude that there are many modes oscillating in the resonator. Between 30 and 55 round trips, on average, the relative amplitude is constant while from 55 round trips the relative amplitude converges to a constant. It can then be concluded that the steady state has been reached. Then the measurements on the steady-state mode were taken (shown in Fig.2.12).

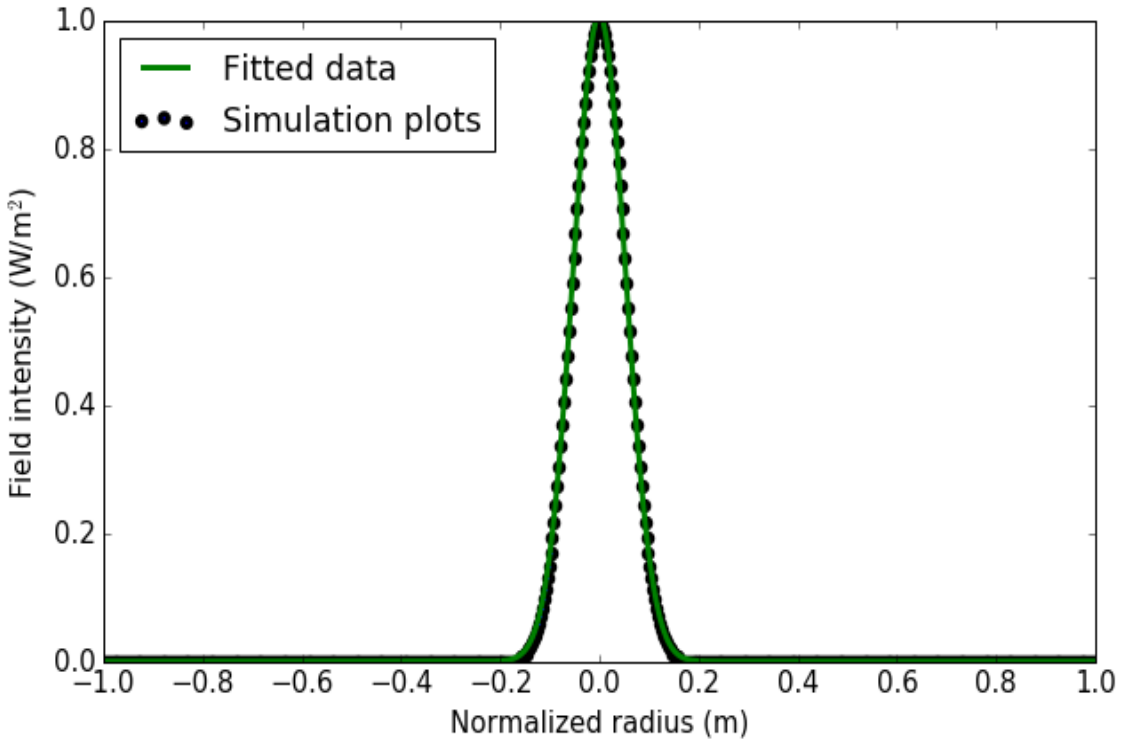


Figure 2.12: Simulation results of a stable cavity with an aperture. Steady-state mode which is Gaussian (black circles) of 211 μm beam size (calculated at $1/e^2$ of maximum intensity) at R_2 mirror is obtained for an aperture size of 320 μm. The plots are fitted with a Gaussian function (green solid line)

Discussion

In the simulation, the steady state was determined to have been reached after 55 round trips and this was seen by comparing successive field distributions. From the results shown in Fig.(2.12), the steady-state distribution is Gaussian as seen from fitting a Gaussian function. From the fitted Gaussian function, the simulation beam radius was measured to be 211 μm. Comparing the simulation results with the theoretical value of 211 μm which was calculated using Eq.(1.15), it was found that the simulation results are in agreement with theory.

2.4.3 Higher order mode

Furthermore, a higher order mode for the same setup as shown in Fig.(2.9) but with an aperture replaced by a loss line (a row or column of zeros in a transfer matrix) of 7 μm thickness was simulated and the result obtained is shown in Fig.(2.13). Similarly, the initial condition is uniform field $|\vec{u^{(2)}}| = 1$ for a wavelength 1064 nm (λ). This was iterated till the steady-state mode was reached which is TEM_{10}. In producing this mode, a loss line was introduced at the central axis($x = 0$).

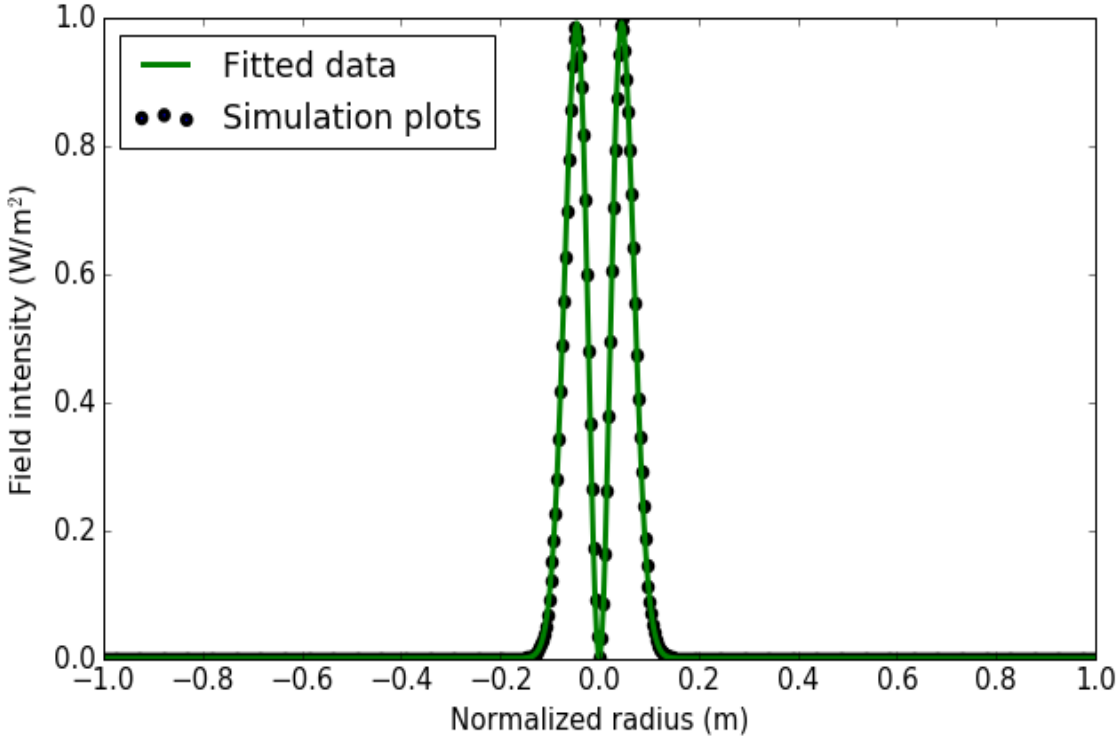


Figure 2.13: Simulation results of a stable cavity with a loss line. Steady-state mode which is TEM_{10} at R_2 mirror is obtained for a loss line at the central axis ($x = 0$) of the mirror. The plots (black circles) are fitted with Hermite-Gaussian function for TEM_{10} mode (green solid line) which is given by Eq.(2.18).

2.5 Summary

In this chapter, numerical methods were used to simulate spatial modes of a passive resonator. The numerical method used is the Fox-Li method which is based on an iterative application of the Fresnel integral.The matrix method modification was principally to speed up the computation process. Applying the matrix method is equivalent to essentially dividing the mirror surface into subdivisions and then followed by applying the Fresnel integral onto those subdivisions. This resulted in the reduction of computation time significantly. The correctness of the free space propagation kernel used in the simulation was tested. This

was done by propagating a Gaussian mode of known initial conditions, then measure beam parameters i.e radius of curvature of a wavefront and beam size, during propagation. Simulation results were then compared to theory using fundamental mode propagation laws. Using the correct propagation kernel, the plano-concave resonator simulations were done. A uniform field was used as the initial condition and an aperture was inserted to select a Gaussian mode as the laser output which is the steady-state field. The results (beam waist) obtained were compared to theory by using equations obtained in chapter 1 for a plano-concave resonator. In addition, higher order mode was simulated by introducing loss lines into the resonator.

Chapter 3

Experimental setup and results

Here a passively Q-switched laser is built and its performance is studied. Q-switched laser output energies are studied for different combinations of Q-switch transmission values and output coupler reflectivities. In addition, the influence of spatial modes on Q-switched pulse shape and pulse width is studied, taking into account the far-field beam divergence of a laser. These laser output features play an important role in range finding applications.

3.1 Flashlamp pumped solid-state laser assembly

3.1.1 Construction overview

From the previous section, it was found that mirror geometry plays an important role in determining the beam waist i.e. gain medium volume utilised. As a consequence, it controls considerably the amount of output energy from a laser. In optimising the laser performance, a plane-parallel mirror resonator was selected which simply means that the whole volume of the gain medium was used since the gain medium was side pumped. Furthermore, spatial mode patterns and corresponding laser pulses were studied. There are two common pump sources used to pump the gain medium, namely, the laser diode and a flashlamp. The former is more efficient in pumping than the latter, this is because the radiation from a laser diode is directional while a flash lamp gives a broad spectrum of radiation [39]. The downside about the laser diodes is that they more expensive than the flash lamp. Since a low-cost laser is designed, a flash lamp was selected as the pump source. Initially, a solid-state laser (long-pulsed operation) is constructed. Then later on, a Q-switch is inserted (Q-switch operation). A schematic diagram of a Q-switched solid-state laser is shown in Fig.(3.1).

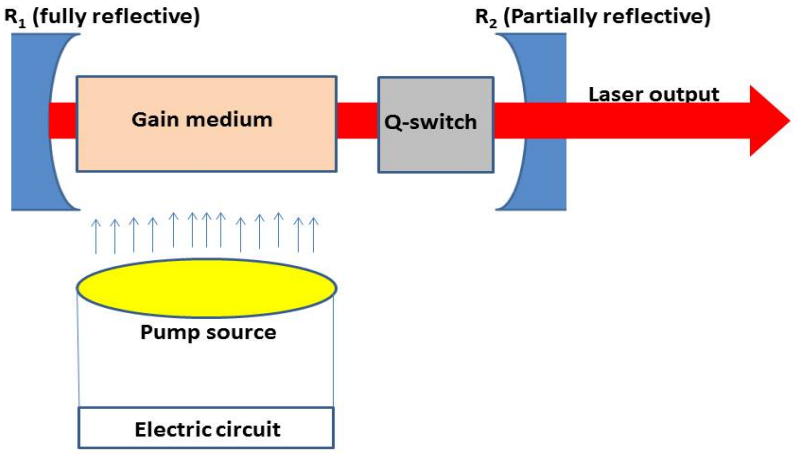


Figure 3.1: Schematic diagram of a passively Q-switched solid-state laser. The electric circuit is used to power the pump source which then excites the gain medium. The Q-switch generates short pulses in the nanosecond regime after saturation, then laser light leaves through partially reflective mirror (R_2).

3.1.2 Laser assembly components

Mirrors

Two Mirrors of unknown optical and geometrical properties were procured (shown in Fig.(3.2)). In quantifying these properties, Lambda900 PerkinElmer spectrophotometer, and Xonox PI500 laser interferometer were used. A range of wavelengths was sent through each mirror ranging from 400-1700 nm by using two light sources, deuterium lamp (400-900 nm) and Tungsten lamp (900-1700 nm). The transmission plots of the results are shown in Fig.(3.3).

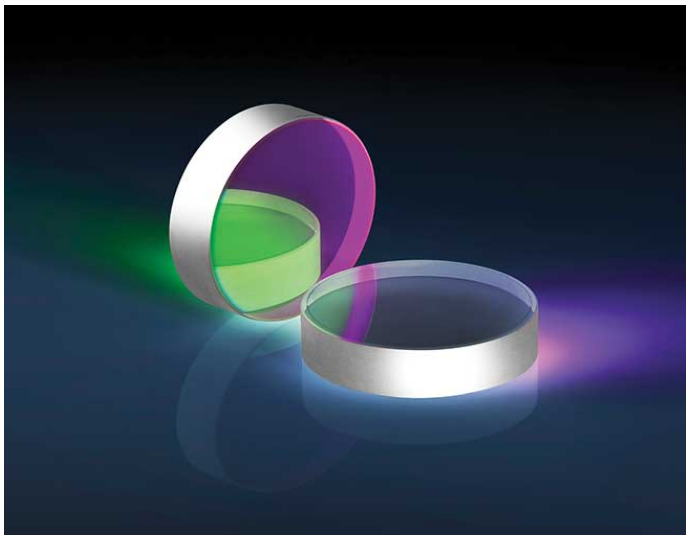


Figure 3.2: A photograph of two coated mirrors (R_2 and R_1) of unknown optical and geometrical properties [40].

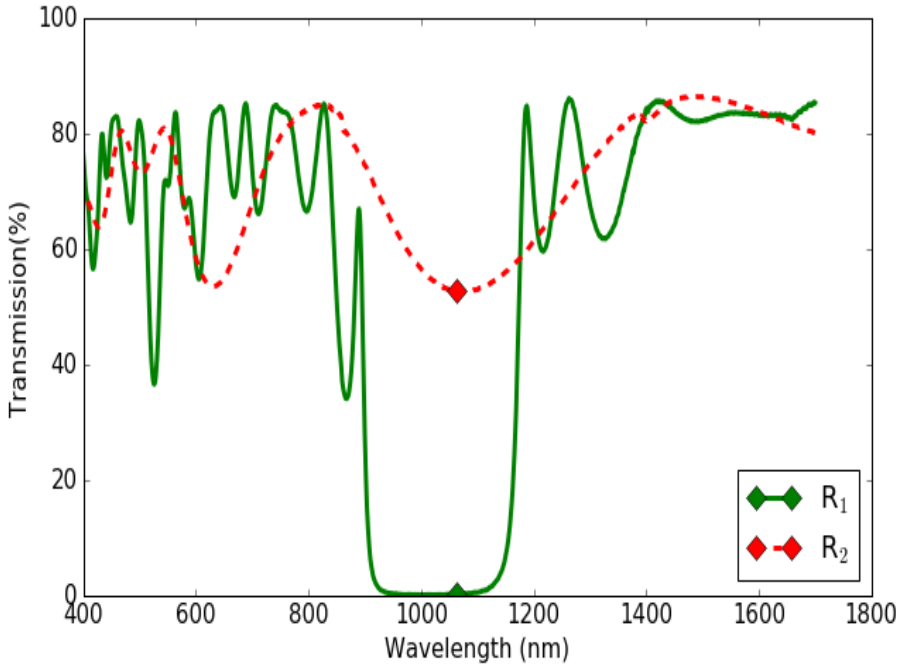


Figure 3.3: The measured transmission of optical wavelength spectra through mirror R_1 (green solid line) and R_2 (red dotted line). The diamond markers for 1064 nm wavelength.

Since the gain medium used was Nd:YAG, which operates in 1064 nm indicated by the markers in Fig.(3.3), mirror R_2 was found to be suitable as the output coupler of 53 % transmission (47 % reflective) and mirror R_1 being $0.13 \approx 0$ % transmissive (100 % reflective) at that particular wavelength. Afterward, the mirrors were taken to the laser interferometer for their geometrical properties to be measured.

The laser interferometer that was used had a flat surface as a reference. Having knowledge about interference pattern of light reflected from top surfaces of reference and tested surfaces, in this case, flat surface and unknown surface respectively, the curvature of the tested surface can be quantified. The theory behind these interferences was studied extensively by Isaac Newton, and thus, the interference pattern from curved surfaces was named Newton's rings in his honour. The results obtained from the interferometer for mirror R_1 and R_2 are shown in Fig.(3.4).

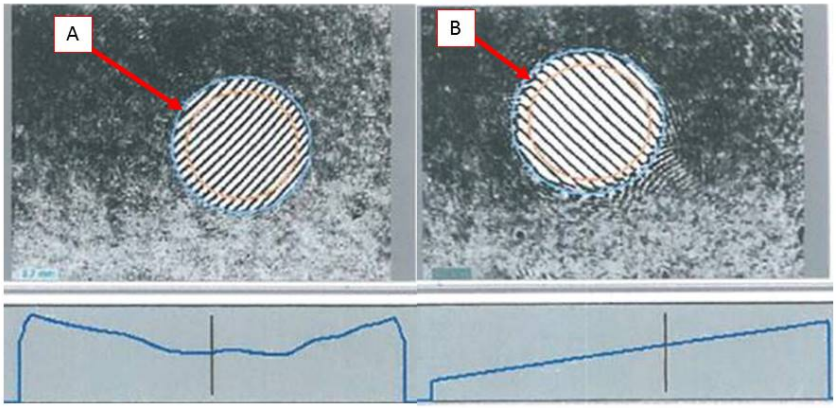


Figure 3.4: The interference pattern and structure of mirrors R_1 and R_2 surface. A and B are interference patterns with corresponding mirror structure indicated by blue traces of mirror R_1 and R_2, respectively.

From Fig.(3.4), looking at the interference which is just parallel lines, it can be concluded that the tested surfaces of mirrors R_1 and R_2 are flat or have a large radius of curvature, hence their structures. The flatness of the mirrors is not perfect, hence the irregularities in blue traces. Additionally, looking at the measured ratio of fringes to radius which are 0.3 and 0.2 for mirror R_1 and R_2 respectively. The radius of curvature of the mirrors can be calculated from [41]

$$R = \frac{r^2}{2t}, \tag{3.1}$$

where r is the radius of the mirror and for constructive interference

$$t = N\frac{\lambda}{4}, \tag{3.2}$$

with N being the order (ratio of fringes to radius) of rings and λ being the interferometer laser wavelength.

Therefore, from the measured ratios of fringes and radius, it is implied that $N = 0.3$ and $N = 0.2$ for mirror R_1 and R_2 respectively. Substituting these and $\lambda = 632.8$ nm of the laser in the interferometer to Eq.(3.2), then substituting the results and using $r = 5$mm to Eq.(3.1), gives $R_1 = 263.4 \approx 263$m and $R_2 = 395.1 \approx 395$m.

Gain and Q-switch medium

In the laser setup, a type of gain medium that was used is a Nd:YAG (neodymium-doped yttrium aluminium garnet) crystal (shown in Fig.(3.5)) where Nd is the dopant and YAG is the host. This particular gain medium was chosen because of its favorable optical, thermal and mechanical properties for solid state lasers [8]. The dimensions of the circular solid Nd:YAG crystal rod used are 4 mm x 50 mm, diameter and length respectively. In generating Q-switched pulses, Cr^{4+}:YAG was used as a Q-switch. The optical properties of these media are shwon in Table (3.1).

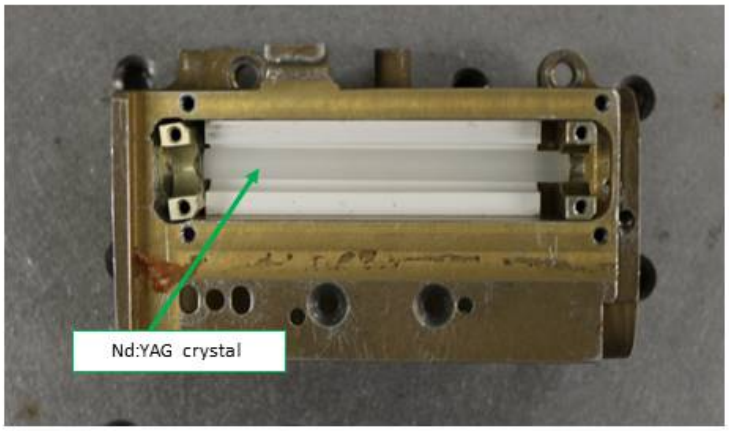


Figure 3.5: A photograph of Nd:YAG crystal used in constructing the laser.

Table 3.1: Optical properties of the Nd:YAG gain medium and Cr^{4+}:YAG Q-switch for σ_{gs} and σ_{es} mentioned in Eq.(1.18).

Media	σ_{gs} (cm^2)	σ_{es} (cm^2)
Nd:YAG		2.2×10^{-19}
Cr^{4+}:YAG	7×10^{-18}	2×10^{-18}

Pump source

The pump source used to excite the gain medium was the Xenon flashlamp. A Xenon flashlamp was used since Xenon is most efficient at converting electrical energy to optical energy and it is easy to trigger. This means it requires low voltages, and thus, is a cheaper pump source. In addition to this, specific regions of the output spectrum of flashlamps can be emphasized by controlling the current through it. This makes it a flexible pump source. But the downside of using a flashlamp as a pumping source is that the best possible pumping configuration in terms of pumping efficiency is side pumping and this configuration in general is less efficient compared to end pumping [42],[39]. This is because side pumping radiation is perpendicular to laser modes. On the other hand, end pumping radiation is parallel to laser modes [39]. The dimensions of the Xenon flashlamp used is 40 and 25 mm body length and arc length respectively and an outer bore diameter of 4 mm. Inductor and capacitor (LC) circuit with a Silicon diode was used to power the flashlamp, the circuit is shown in Fig.(3.6).

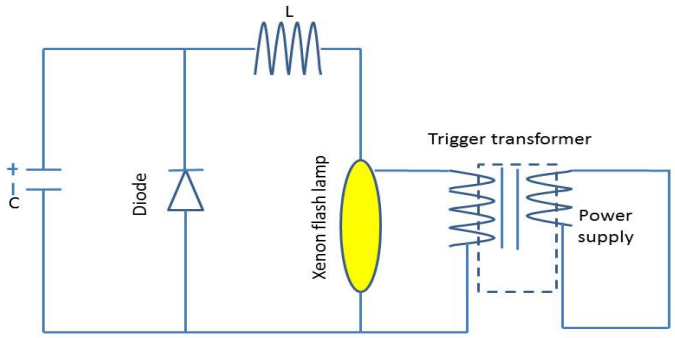


Figure 3.6: A schematic of the LC circuit used to power Xenon flashlamp. The capacitance (C) of C= 20μF was used for the circuit. An in-house developed test transmitter (power supply) unit was used to drive the LC circuit.

The current pulse that transfers energy from the capacitor to the flashlamp was then measured (shown in Fig.(3.7)).

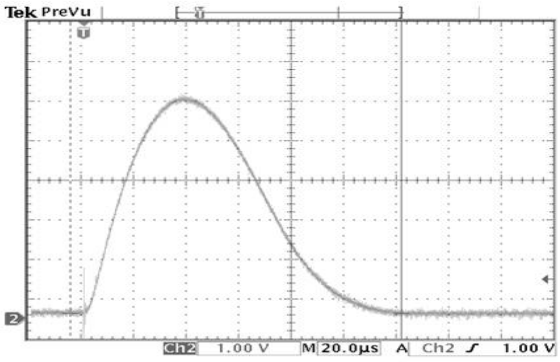


Figure 3.7: An oscilloscope trace of the current pulse applied to the Xenon flashlamp.

From Fig.(3.7), it can be seen that energy from a capacitor is transferred to the flashlamp in a critically damped pulse (fast decaying pulse without oscillation), and this was made possible by the diode in the circuit. Since the diode only allows the current to move through it in one direction, there is no reversal of current. As a consequence, energy is transferred most efficiently from a capacitor to the lamp. A pump cavity encasing both flashlamp and the gain medium (as shown in Fig.(3.8)) was used to further improve pumping efficiency of Xenon flashlamp by internally reflecting light emitted by the flashlamp. The casing was air cooled. The pump cavity used was rectangular and made up of white aluminum oxide (Al_2O_3) of 46x12x17 mm^3 volume dimensions and inner vertical oval hole of 46x6x9 mm^3 volume of 5 mm radius of curvature at both ends.

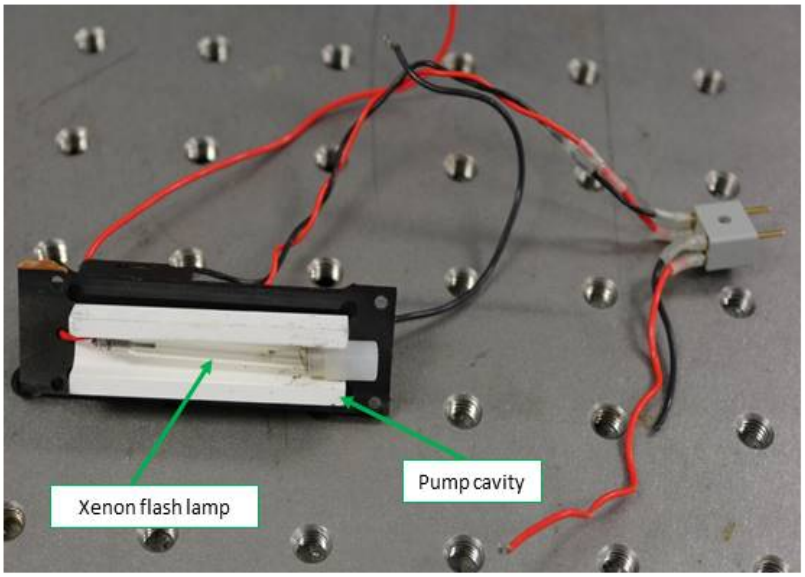


Figure 3.8: A photograph of Xenon flash lamp (transparent) and one side of pump cavity (white in colour).

3.1.3 Complete laser assembly

Knowing the optical and geometrical properties of the optics that were used to build a laser allows us to assemble and align all the optics as shown in Fig.(3.9). In assembling the optics, the distance between the two mirrors was kept as short as possible (80 mm) while taking into account the distance needed for fine adjustments on the mirrors. This was done to optimise laser performance i.e high output energies and short pulses.

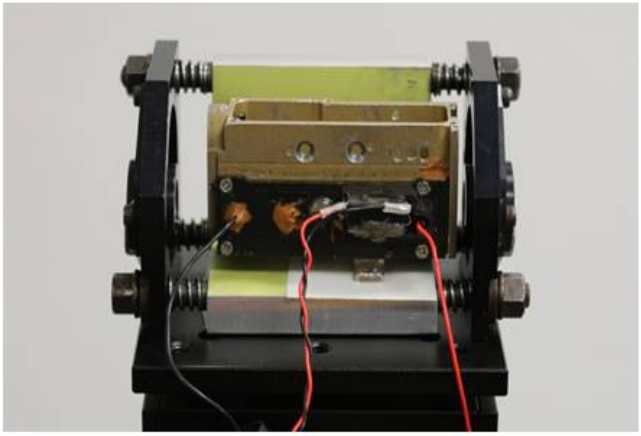


Figure 3.9: A photograph of an assembled Nd:YAG laser setup. The geometrical length of cavity (length between two mirrors) of 80 mm

In building the Nd:YAG laser shown in Fig.(3.9) as part of the experiment, it was necessary to first define an optical axis by using a visible laser light (e.g the red laser) passing through the gain medium. Then the gain medium was orientated in such a way that the reflected light superimposes onto the incident laser light. The plane mirrors were then inserted and also oriented to the optical axis in a similar fashion as the gain medium. Afterward, the Nd:YAG solid-state laser was switched on, operating in 1 Hertz and the mirrors were further fine-tuned to optimise the laser performance i.e symmetrical transverse mode pattern while simultaneously obtaining high output energy. The entire setup of the laser and measuring instruments used is shown in Fig.(3.10)

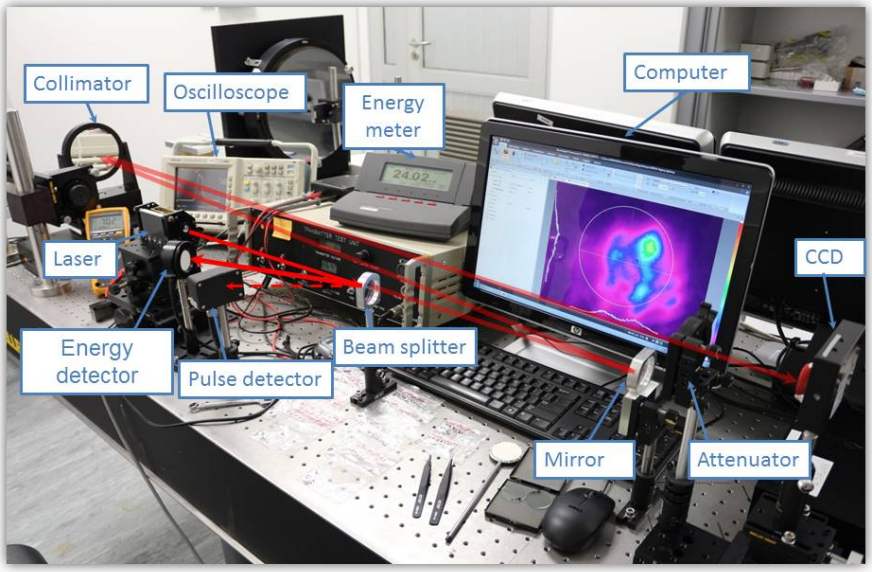


Figure 3.10: A Photograph of the experimental setup to generate a Q-switched pulse from a laser and capture transverse mode patterns at the far field with their corresponding generated pulse and output energy. The laser light coming from a laser is split by the beam splitter which is orientated at an angle where 99 % of the reflected light is directed to the energy detector connected to the energy meter. The pulse detector is connected to the oscilloscope alongside the beam splitter. The remaining 1 % of the laser light gets transmitted to a flat mirror, then reflected to the collimator of 1542 mm focal length for far field projection. The reflected light from the collimator is then captured by the CCD beam profiler which connected to the computer and placed at the focal length of the collimator.

In the experiment, an in-house developed test transmitter unit was used to drive the pump head for the time interval of 3 minutes between flashlamp pumping. Electrical input energy into a flashlamp was varied by changing the voltage from 405 V to 705 V through increments of 20 V. The energy stored in the capacitor is given by $E = \frac{1}{2}CV^2$ [8], where the capacitance of $C = 20\mu$F was chosen for flashlamp circuit. A Fluke 175 digital multimeter was used to measure the voltage. The corresponding laser output energies were then detected by PE50BF-DIF-V2 P/N 7Z02888 pyroelectric detector connected to the Ophir P/N 7Z01600 laser star energy meter.

3.2 Output performance

3.2.1 Output energy

Long-pulsed operation results

Long-pulsed (no Q-switch in the resonator) energy measurements read from the energy meter were recorded and the results were plotted as shown in Fig.(3.11) for the output coupler of 47 % reflectivity.

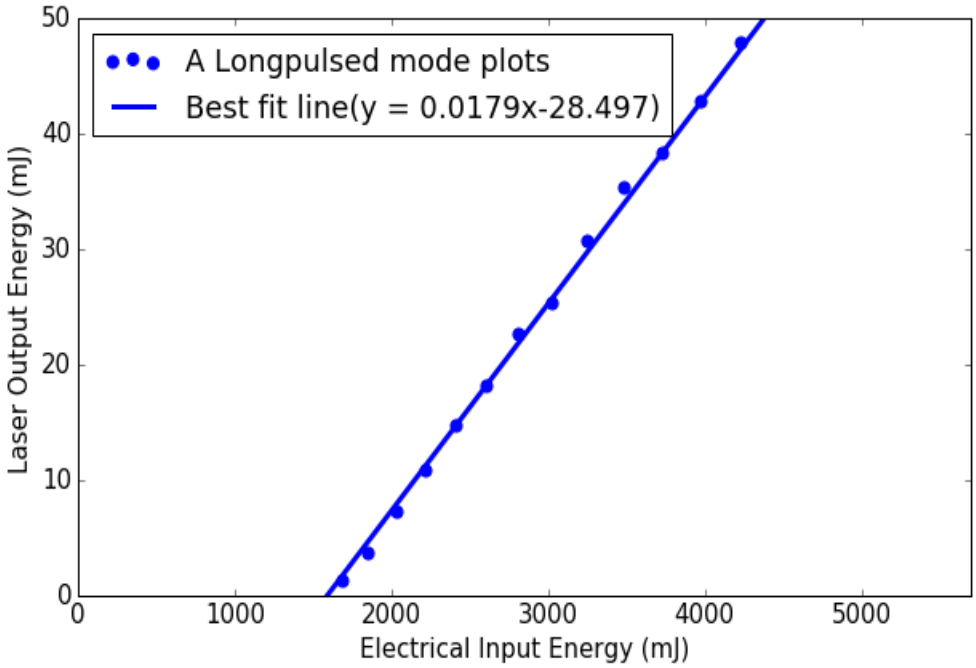


Figure 3.11: Experimental plots of an Nd:YAG laser in long-pulsed operation and solid line of best fit.

In long-pulsed operation, threshold energy, slope, pumping and extraction efficiencies were calculated.

From the equation of the line of best fit, threshold energy and slope efficiency were determined to be 1592 mJ and 1.79 %, respectively. Using long-pulsed n_i calculated from Eq.(1.19), where in long-pulsed operation $T_0 \equiv 100\%$ since there is no Q-switch, stored energy was calculated from Eq.(1.23) to be 42.65 mJ. Then, pumping efficiency (ratio of stored energy to threshold energy) was determined to be 2.68 %. Using the ratio of pumping efficiency to slope efficiency, extraction efficiency was calculated to be 1.50 %. A different reflectivity of output coupler was used to determine the effect on the threshold and slope efficiency of the laser.

In extensively studying the effect of reflectivity, output couplers of lower and higher reflectivity than 47 % were chosen. Output couplers of 40 and 70 % reflectivity were used, and the results were plotted as shown in Fig.(3.12).

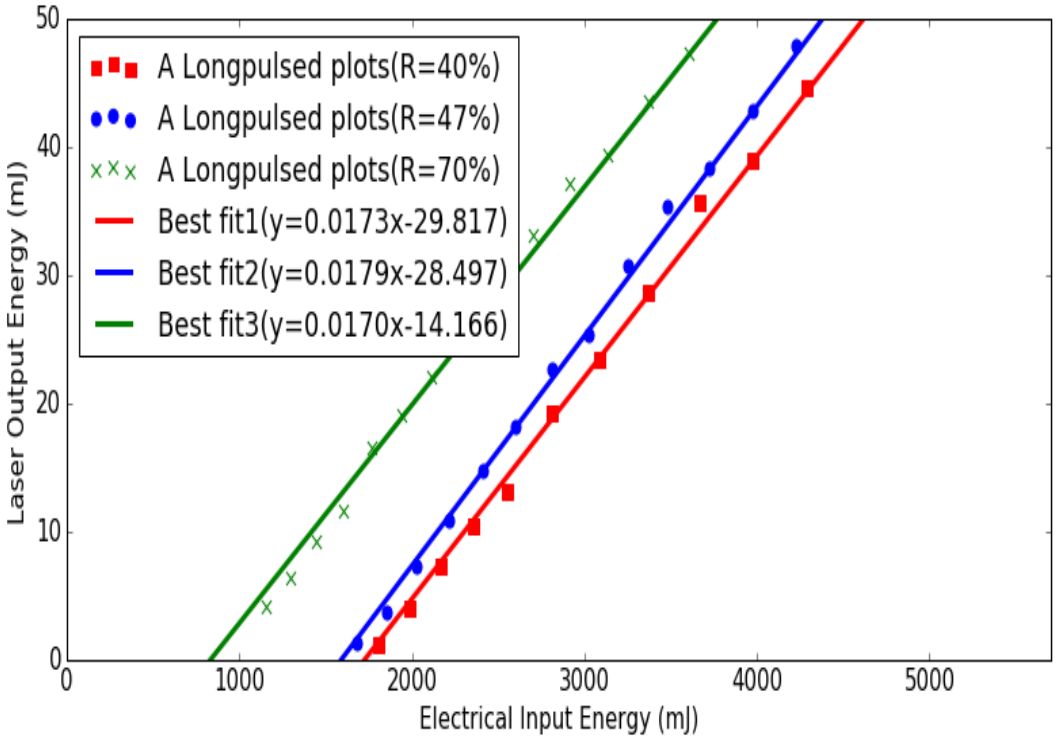


Figure 3.12: Experimental plots of an Nd:YAG laser in long-pulsed operation for different reflectivity output couplers and their respective solid lines of best fit. Plots for the reflectivity of 40, 47 and 70 % indicated by green stars, blue circles, and red squares markers, respectively. Together with their lines of best fit of corresponding colours to their markers.

From the equations of a line of best fit for output coupler of 40 and 70% reflectivity, threshold energy and slope efficiency were determined. The threshold energies were calculated to be 1724 mJ and 833 mJ, and slope efficiencies were determined to be 1.73% and 1.70% for the reflectivity of 40 and 70%, respectively.

Discussion

From the plot in Fig.(3.11), it can be seen that there is a linear relationship between electrical input energy and laser output energy, which correlates to the theoretical prediction [8]. The experimentally obtained slope efficiency of 1.79 % was found to be within a reasonable range since the literature value of a similar pump cavity has a slope efficiency of 2 % for Krypton lamp [8]. The difference of 0.21 % can be attributed to the fact that Krypton lamp acts as a better match to the absorption spectra of Nd:YAG crystal than the Xenon lamp [8], [43]. This slope efficiency is essentially the product of all the efficiencies in the resonator, pump efficiency, transfer efficiency, absorption efficiency, upper state efficiency, beam overlap efficiency and extraction efficiency. In theory, each efficiency can be calculated. The use of a flashlamp as a pump source increases the difficulty in evaluating each efficiency in an experiment since a flashlamp output spectrum is broadband. Long-pulse slope measurement is crucial since it is used together with threshold energy to give a relation between electrical input energy and stored energy i.e. pumping efficiency, in the laser rod. This can be used

in Q-switch operation since the pumping efficiency of the laser rod is constant. Also, in long-pulse mode, extraction efficiency can be determined by using pumping efficiency and slope efficiency.

In Fig.(3.12), it was seen that the mirror reflectivity has no effect on the slope efficiency of a laser since for reflectivity of 40,47 and 70 %, slope efficiencies of 1.73, 1.79 and 1.70 % respectively, were obtained. On the other hand, as the mirror reflectivity was increased, low threshold energy was required to initiate lasing and vice-versa. For example, from the reflectivity of 47 to 70 % resulted in threshold energy of 833 mJ from threshold energy of 1592 mJ. The results are reasonable since slope efficiency is a ratio of stored and pumping energy, and by changing mirror reflectivity, only different losses are introduced, therefore different threshold conditions but same slope of stored and pumping energy.

Q-switch operation results

In Q-switch operation, three Q-switches of different transmission values were used to evaluate the effect of a Q-switch transmission on the threshold and output energy of the laser. These Q-switch initial transmission values are 40,53 and 65 % and were used on the selected three output coupler reflectivity, 40, 47 and 70 %. Initially, the selected Q-switch transmissions values were used for an arbitrary reflectivity mirror of 47 %. This was chosen since 40 and 70 % reflectivity mirrors would result in no lasing and multiple pulses for some Q-switches, respectively. After selecting the 47 %, then passive Q-switch behaviour with respect to electrical input energy was studied even beyond threshold energy (as shown in Fig.(3.13)).

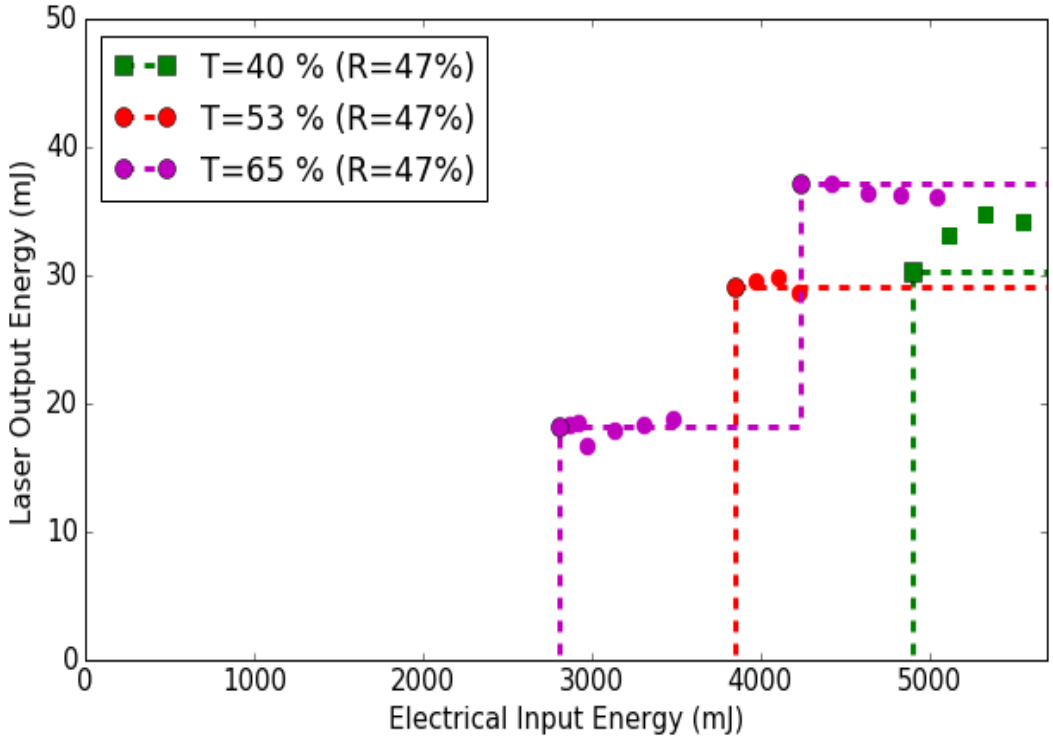


Figure 3.13: Experimental plots of a Q-switched Nd:YAG laser using different Q-switch transmission values and step dashed lines were drawn to fit the plots. Q-switch transmission values of 40, 53 and 65 % were used and their plots are indicated by purple circles, red circles, and green square markers, respectively.

From Fig.(3.13), it was noticed that a passively Q-switched laser gives, on average, constant output energy even when electrical input energy is beyond threshold energy. This behaviour is due to the nature of a passive Q-switch. The passive Q-switch is a saturable absorber, and thus, saturates only at particular intensity of light. Furthermore, this was also observed for the Q-switch of 65 % transmission where a second threshold (2nd pulse) was reached, as seen from doubling of the output energy; below the saturation condition, it results in constant output energy. Therefore, from now onwards, only the threshold energy was used for the plots. The results for all selected reflectivities were then plotted in Fig.(3.14).

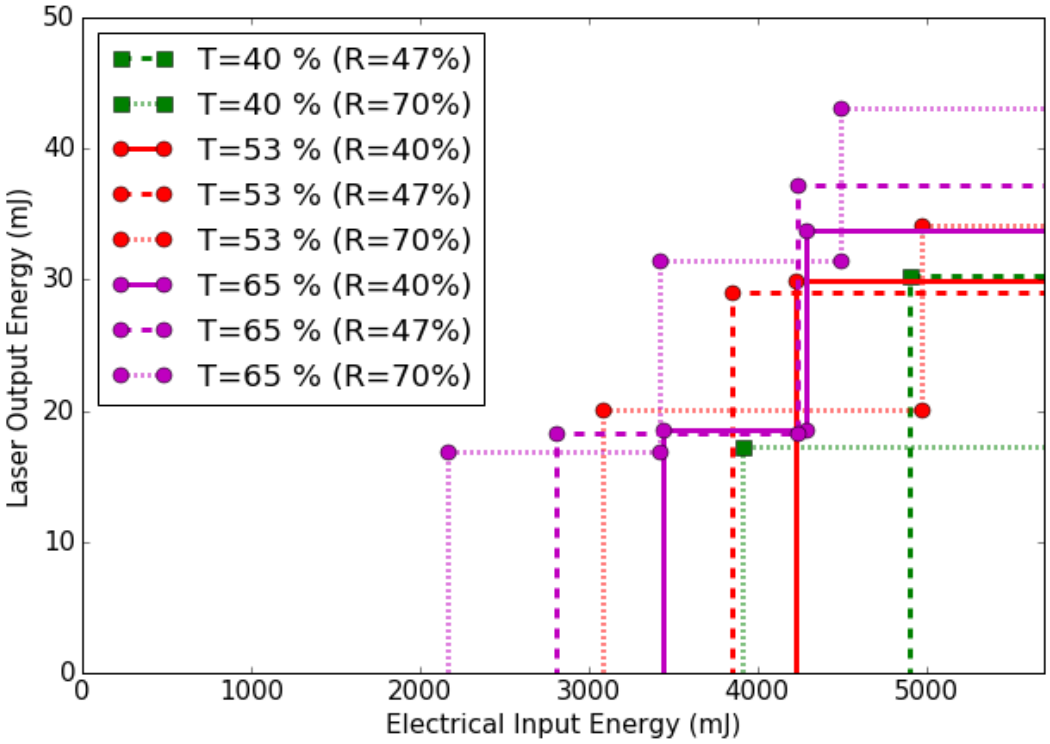


Figure 3.14: Experimental plots of a Q-switched Nd:YAG laser using different Q-switch transmission values per mirror reflectivity and step lines drawn to fit the plots. Q-switch transmission values of 40, 53 and 65 % were used and these are indicated by green squares, red circles and purple circles, respectively. Mirror reflectivity of 40, 47 and 70 % indicated by solid line, dashed line and dotted line, respectively.

The results were then compared to theoretically calculated values using Eq.(1.22). The experimental and theoretical values are tabulated in Table (3.2). In the calculations, the optical properties of the Nd:YAG and Cr^{4+}:YAG media given in Table (3.1) and resonator losses of $L = 1.7\%$ were used. This value was obtained from summing reflection losses per round trip which are due to laser radiation interaction with gain medium(0.8 % per round trip), Q-switch (0.8 % per round trip) and highly reflective mirror (0.13 %). The $\gamma = 2$ was chosen since short pulse which is comparable to the lower excited state relaxation time (30 ns) of the gain medium was generated [19],[31].

Table 3.2: Comparison of experimental and theoretical output energy using different Q-switch transmission values (Cr^{4+}:YAG properties given in Table (3.1)) per mirror reflectivity.

Reflectivity (%)	Q-switches (%)	Experimental E_{out} (mJ)	Theoretical E_{out} (mJ)
40	40		
	53	31	26
	65	20	20
47	40	35	30
	53	30	24
	65	19	19
70	40	21	20
	53	20	17
	65	17	14

The discrepancy between the experimental and theoretical results in Table (3.2) was observed, and this is discussed under discussion section. As a result, different optical properties of the Q-switch were used. The guessed (iteratively changed variable to find a better agreement with theory) variables are $\sigma_{gs} = 5 \times 10^{-18}$ cm^2 and $\sigma_{es} = 1 \times 10^{-18}$ cm^2 for the Cr^{4+}:YAG Q-switch at 1064 nm wavelength, and the results are shown in Table (3.3).

Table 3.3: Comparison of experimental and theoretical output energy using different Q-switch transmission values (guessed properties) per mirror reflectivity.

Reflectivity (%)	Q-switches (%)	Experimental E_{out} (mJ)	Theoretical E_{out} (mJ)
40	40		
	53	31	31
	65	20	23
47	40	35	36
	53	30	29
	65	19	22
70	40	21	25
	53	20	21
	65	17	17

Discussion

In Fig.(3.13), the reflectivity of the mirror was kept constant (47 % reflectivity) and only the Q-switch transmission values were changed. The results obtained show that for the Q-switch of lower transmission, high threshold energies were required and vice-versa. For example, Q-switch transmission of 53 and 65 % required threshold energies of 3848 mJ and 2809 mJ, respectively. On the output energies, Q-switch of lower transmission was found to give high output energy. Comparing energies in a single pulse, a Q-switch of 53 and 65 % gave output energies of 30 mJ and 19 mJ, respectively. In Fig.(3.14), looking only at the output energies for a single pulse, combinations of Q-switch transmission of 53 % and 40 % for mirror reflectivity of 47 % give high output energy results compared to other combinations. Furthermore,

the difference between output energies of Q-switch 53 and 40 % transmission is not too large, namely, 30 and 35 mJ compared to their threshold energy difference of 1052 mJ (from 3848 and 4900 mJ), respectively. Therefore, a combination of 53 % Q-switch transmission and mirror reflectivity of 47 % give an optimised laser performance considering both, threshold energy and output energy.

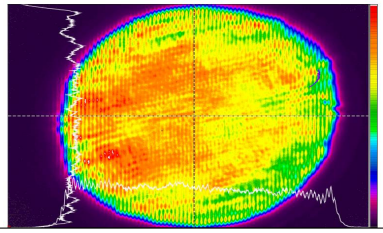
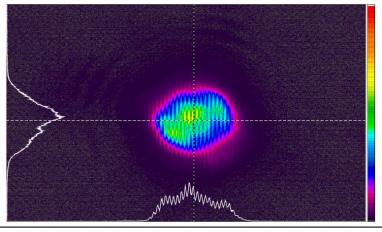
In Table (3.2), properties used for the Q-switch are from literature [8]. For some results in Table (3.2) there is a significant discrepancy between experimental results and theory, for example, for mirror reflectivity of 40 % and Q-switch transmission of 53 %, the results of the output energy from the experiment and theory are 31 and 26 mJ and therefore have a discrepancy of 5 mJ. This discrepancy may be due to an incorrect assumption on properties of the Q-switch used in the experiment. Literature properties were assumed to be the correct properties of the Q-switch used in the experiment. It is also mentioned from articles that properties of the Q-switch are somewhat controversial in a sense that different sources give different values[44], [27]. As a result, it gave us the freedom to use Q-switch properties instead of active medium to guess appropriate σ_{gs} and σ_{es} that would match the experiment. In Table (3.3), the properties of the Q-switch were guessed using a trial-and-error method, and the theoretical results were found to be in good agreement with the experiment.

3.2.2 Spatial mode results

In studying spatial mode, a plano-concave resonator was used. This is done by replacing a flat output coupler with a curved output coupler of 5 m radius of curvature and 62 % reflectivity at 1064 nm wavelength. Initially, a plano-concave resonator with no aperture inserted was studied. Later on, the aperture was then inserted to study the influence of modes to a Q-switch pulse and this was done by capturing spatial modes corresponding to Q-switch pulses.

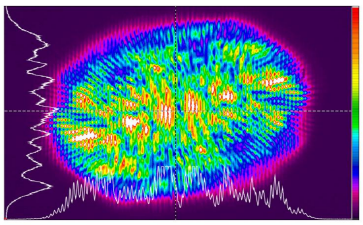
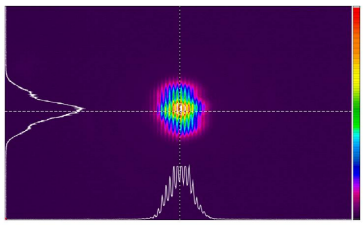
long-pulsed operation

Table 3.4: Captured far field Nd:YAG laser spatial mode pattern with varying aperture size and corresponding full beam divergence.

Properties measured	No aperture	1 mm diameter aperture
spatial mode		
Full beam divergence (mrad)	18.50	6.05

Q-switched operation

Table 3.5: Captured far field Q-switched Nd:YAG laser spatial mode pattern with varying aperture size and corresponding full beam divergence.

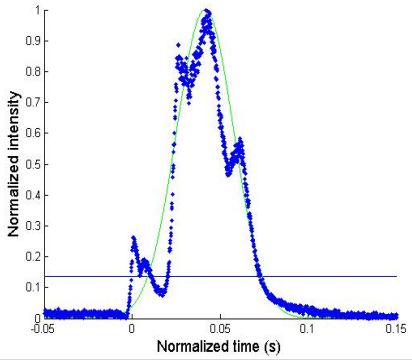
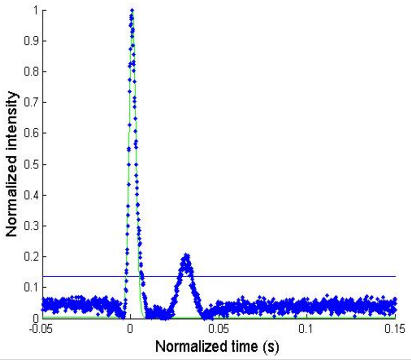
Properties measured	No aperture	1 mm diameter aperture
spatial mode		
Full beam divergence (mrad)	17.18	5.29

Discussion

Looking at Table (3.4) and Table (3.5) for both long-pulsed and Q-switched operation, as beam diameter was decreased by inserting an aperture, the beam divergence also decreased. Also, the number of modes as the laser output got reduced as seen from the reduction of the beam quality (the product of full beam divergence and beam diameter). In comparing Q-switched operation results with long-pulsed operation results, it was observed that a Q-switched laser gives fewer modes as the output than in long pulsed operation for the same resonator setup. This can be observed from obtaining smaller beam divergence in Q-switched operation for a given beam diameter. For example (from table 3.4 and 3.5) for a beam of 1 mm diameter aperture, beam divergence in long-pulsed and Q-switched operation are given by 6.05 and 5.29 mrad, respectively. This is reasonable since in Q-switch operation, due to rapid Q-switching (faster than in long-pulsed operation), some modes do not get enough time to reach the threshold point. Comparing spatial modes in a long-pulsed and Q-switched operation when there is no aperture, shows that in a Q-switched laser, the spatial mode is not as uniform as in long-pulsed. This can be attributed to the poor surface quality of the Q-switch, such as surface roughness, and this may result in obtaining fewer modes as a laser output since areas of poor quality on a Q-switch introduce additional losses. This means that more gain is required to reach threshold.

3.2.3 Q-switched temporal mode results

Table 3.6: Detected Q-switched pulse with varying aperture size fitted with Gaussian profile and the corresponding pulse width.

Properties measured	No aperture	1 mm diameter aperture
Temporal mode		
Pulse width (ns)	50	6

Discussion

The results in Table (3.6) are the corresponding pulses to the spatial modes in Table (3.5). In Table (3.6), when there is no aperture an irregular pulse compared to a Gaussian fit curve of 50 ns pulse width was obtained. After inserting an aperture of 1 mm diameter, a smoother pulse of 6 ns pulse width along with a small second pulse often referred to as a satellite pulse was obtained. As discussed from the previous section, a reduction in the beam diameter resulted in the number of modes being reduced. The changes in pulse shape and pulse width are also attributed to spatial modes. In the case when there is no aperture, the pulse width is large due to different modes reaching their threshold point at different times [45], and thus, for fewer modes (when the aperture is inserted), a short pulse is obtained. There are, however, drawbacks in producing this short pulse in a stable resonator. A significant loss of output energy due to losses introduced by aperture and production of a satellite pulse is experienced. A satellite pulse is produced from gain recovery after producing the main pulse.

3.3 Summary

In this chapter; the spatial modes' influence on pulse width, pulse shape and beam divergence were studied; and optimisation of laser output energies. In optimisation of laser output energies, different combinations of Q-switch transmission values and output coupler reflectivities were used and the results were compared to theory. For each output coupler reflectivity tested, effects of the Q-switch transmission value on output and threshold energy was studied. Then, looking at both output and threshold energy, a particular combination of Q-switch transmission value and output coupler was selected. In studying the influence of

the spatial modes on pulse shape, pulse width and beam divergence, an aperture was used to reduce the number of spatial modes by introducing energy losses.

Chapter 4

Conclusions and Future work

4.1 Conclusions

The first chapter focused on laser principles and resonator configurations discussion; achieving those principles: absorption, spontaneous and stimulated emission required thorough discussion on various pumping sources and gain media. Any one of the available pumping sources and gain media can be chosen depending on the performance requirements of a laser. Likewise, a particular resonator configuration can be chosen depending on the required laser performance, as an example, a plano-concave resonator was chosen to mathematically show how Gaussian beam parameters change with resonator parameters.

In the second chapter, numerical methods were used to simulate spatial modes of a passive resonator. The numerical method used is the Fox-Li method which is based on an iterative application of the Fresnel integral.The matrix method was incorporated to modify this method. Applying the matrix method is equivalent to essentially dividing the mirror surface into subdivisions and then followed by applying the Fresnel integral onto those subdivisions. The correctness of the free-space propagation kernel used in the simulation was tested. This was done by propagating a Gaussian mode of known initial conditions, then measure beam parameters i.e. radius of curvature of a wavefront and beam size, during propagation. Simulation results were then compared to theory using fundamental mode propagation laws. Using the correct propagation kernel, the plano-concave resonator simulations were done. A uniform field was used as the initial condition and an aperture was inserted to select a Gaussian mode as the laser output which is the steady-state field. The results (beam waist) obtained were compared to theory by using equations obtained in chapter 1 for a plano-concave resonator. In addition, higher order mode was simulated by introducing a loss line into the resonator. From the simulation results obtained, it can be concluded that the Fox-Li method was successfully able to develop spatial modes that are obtained in laser resonators by taking into account diffraction effects caused by the optics. This method was only applied in a passive resonator in one dimension. For advanced resonators taking into account optics inside the resonator, the general form of Fresnel's integral which is Collin's integral, can be used.

In the final experimental chapter, Q-switched laser output energies and the spatial modes influence on pulse width, pulse shape and beam divergence were studied. In the study of Q-switched laser output energies, different combinations of Q-switch transmission values and output coupler reflectivities were used and the results obtained were compared to theory. For each output coupler reflectivity tested, the effects of the Q-switch transmission value on output and threshold energies were studied. Then, looking at both output and threshold energies, a particular combination of Q-switch transmission value and output coupler was selected. In studying the influence of the spatial modes on pulse shape, pulse width and beam divergence, an aperture was used to reduce the number of spatial modes by introducing energy losses. From the results obtained, it can be concluded that a plane-parallel resonator is better in terms of laser output energies. The spatial modes of a laser were found to dictate both pulse shape and pulse width. This influence of spatial modes on a laser pulse was also observed in other articles of a similar laser setup.

The initial plan was to try out different combinations of Q-switch transmission and output coupler reflectivity to find the optimum combination which would then be used to build a monolithic version to further reduce the cost. But due to time delay caused by the unreliability of Q-switch properties when trying to match theoretical and experimental results, we could not realise our plan. But, despite that, the results obtained here can still be used as a guide to pursue a monolithic design version of a passively Q-switched laser. The first step towards building a monolithic design by using the analysis obtained in the previous chapter has been presented in the next section.

In comparing the results obtained here with other current designs of similar setup, it was found challenging as there is some differences regarding parameters used such as pump sources and pumping configurations. In other designs, they use laser diodes as their pumping sources and also pump the crystal from its end (end pumping).

4.2 Future work

Here, the analysis obtained from the previous chapter regarding laser output energy and spatial modes influence on pulse shape and pulse width was considered. As a result, for an optimum laser output, a plane-parallel resonator i.e high laser output energies, was chosen. But now focusing on the pulse shape, pulse width and their corresponding beam divergence since these are important parameters in range finding application. The preliminary results obtained are discussed in the next sub-section. Later on, the laser design was improved by using a samarium flow tube.

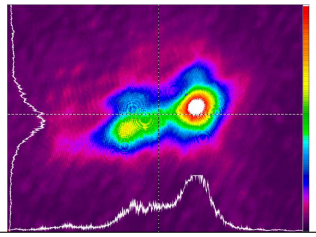
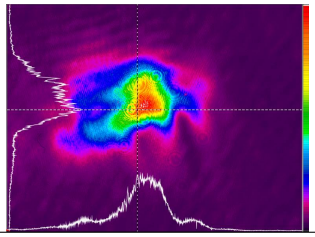
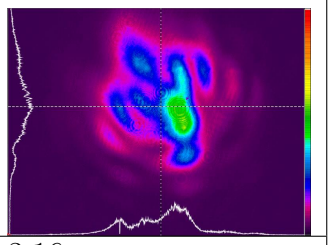
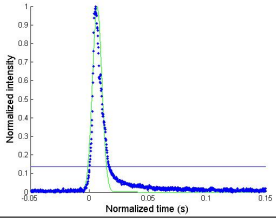
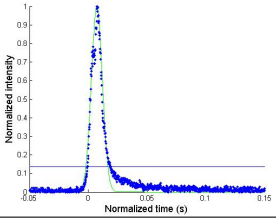
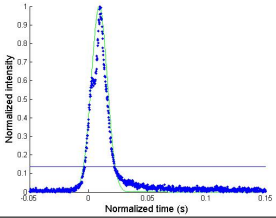
4.2.1 General modal analysis (time and space)

In previous sections, it was found that to achieve a short smooth pulse in a plano-concave resonator, sacrifices in output energies had to be made. On the other hand, a plane-parallel resonator gave optimised output energies, in particular, for a mirror of 47 % reflectivity in Q-switch operation. As a result, here a plane-parallel resonator without an aperture was

chosen so to study the Q-switch spatial modes together with their corresponding pulses. All three Q-switch transmissions, namely, 40,53 and 65 % were studied for the mirror of 47 % reflectivity. The results are tabulated in Table (4.1).

Results

Table 4.1: Captured far field Q-switched spatial mode pattern with corresponding pulse generated and measured full beam divergence and pulse width for different Q-switch transmission values.

Beam properties	Q-switch transmissions (%)		
	40	53	65
Spatial modes			
Full beam divergence (mrad)	3.40	3.15	3.16
Temporal mode			
Pulse width (ns)	8	10	14

Discussion

In Table (4.1), spatial modes with their corresponding pulses are shown. In the plane-parallel resonator, it was found that short pulses, for example, of 8 ns pulse width were generated without the aid of inserting an aperture. In addition, a laser beam of small beam divergence of approximately 3 mrad was produced despite non-uniformity of spatial mode. The non-uniformity of a spatial mode is attributed to Q-switch surface quality as seen from table 4.1 that for different Q-switches for the same resonator setup, a different spatial mode distribution is obtained. Also, as discussed in previous sections, spatial modes dictate pulse shape and pulse width. This is also noticed in table 4.1 when looking at the pulse shape and pulse width of the corresponding pulses produced.

4.2.2 Improvements to laser design

In a Q-switched laser, before Q-switching, there are losses caused by Amplified Spontaneous Emission (ASE) and fluorescence which depopulate the inversion population on the upper

excited state in the laser medium. So to reduce those losses, we use a Samarium-doped glass flow tube around the Nd:YAG laser rod. The Samarium-doped glass flow tube absorbs the spontaneously emitted 1.064 μ photons from the ASE process, and thus, prevents the depopulation of the upper state stored energy.

Then we check the effect of the Samarium-doped glass flow tube on laser threshold energy i.e. effect of amplified spontaneous emission. In checking the Samarium flow tube effect surrounding the laser rod on the laser output energy, a setup of an experiment is prepared in which there is no flow tube and then the same setup is repeated but now with a flow tube in the setup. For this setup, a new pump cavity that enables a samarium flow tube to fit was used. In both set-ups, threshold energy measurements are taken and then are compared, the results are shown in Fig.(4.1).

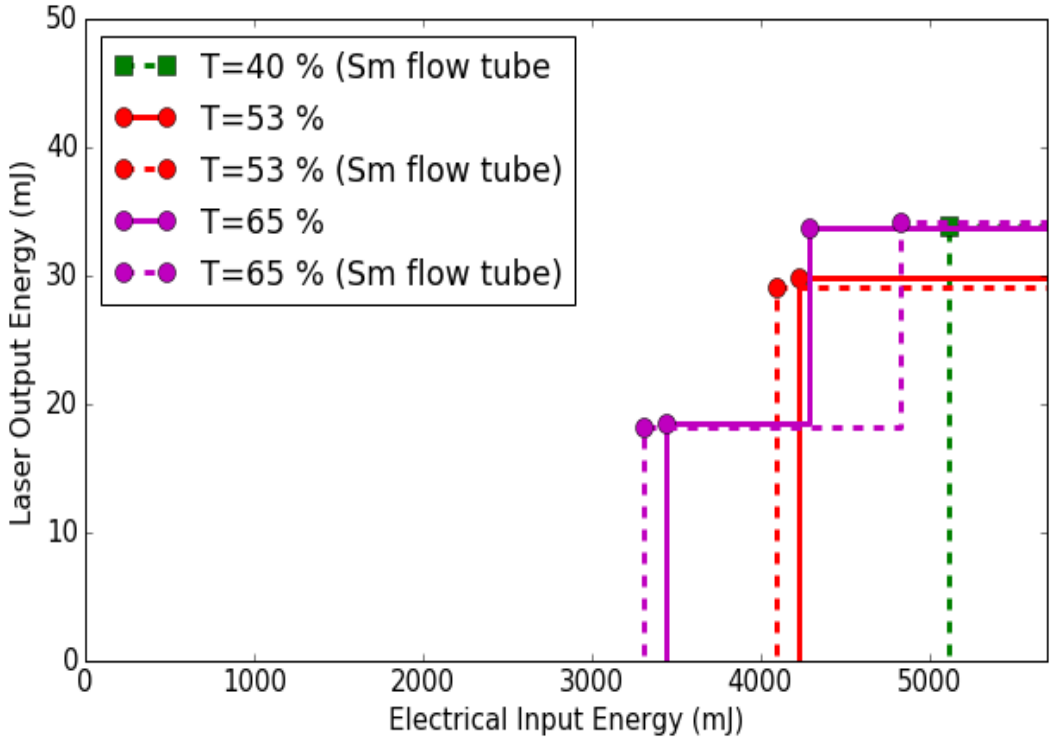


Figure 4.1: Experimental plots of a Q-switched Nd:YAG laser for a setup with and without a Samarium flow tube for different Q-switch transmission values, and step lines fitted to the plots. Dashed lines and solid lines presenting a setup with and without a Samarium flow tube, respectively. Q-switch transmission values of 40, 53 and 65 % indicated by green squares, red circles and purple circles markers, respectively.

Discussion

From Fig.(4.1), it was observed that when Samarium flow tube was inserted, lower threshold energies were required to initiate lasing. For an example, a Q-switch of 53 % transmission value without a Samarium flow tube required energy of 4230 mJ, but with a Samarium flow

tube inserted, a threshold energy of 4100 mJ was required to initiate lasing. Therefore, 3 % less energy was used to initiate lasing. Therefore, the effect of a Samarium flow tube on amplified spontaneous emission was demonstrated. Furthermore, for the 40 % Q-switch transmission which could not lase without a Samarium flow tube, when a Samarium flow tube was inserted, it did lase, hence a green dashed line in Fig.(4.1).

Suggestions on further improving laser performance

Looking at the experimental spatial mode distributions captured by the CCD beam profiler in Q-switch operation, it was observed that the spatial mode distributions are not uniform. As discussed in previous sections, it is because of the surface quality of the Q-switch. Therefore, a laser performance can be further improved by using a Q-switch having a good surface quality. This means that less threshold energies would be required to initiate lasing.

Also, numerical methods originally discussed by Degnan to optimise a Q-switched laser can be used in selecting a good combination of Q-switch transmission value and a mirror reflectivity that can give an optimised laser performance by using energy extraction efficiency strategy [19]. The optimisation is based upon looking at laser output energy then applying Lagrange multipliers to solve the obtained equation [46]. But it should be noted that in Degnan's paper, losses due to excited state absorption of a Q-switch are not taken into account. Therefore, for Cr^{4+}:YAG, these losses need to be taken into account. It is thus advantageous to use a modified version of Degnan's equation. These are given in Liu's paper [31].

Ultimately, building a monolithic version of the Q-switched laser (the Q-switch and laser rod fused together into a single unit) of optimum combination of Q-switch transmission value and mirror reflectivity would greatly improve the design. This reduces costs and makes the design to be much simpler to handle since no alignments would be required everytime a laser needs to be used [47]. This would be ensured by polishing the mirror at the ends of the Q-switch and laser rod.

Bibliography

[1] W. T. Silfvast, "Laser fundamentals,". Cambridge University Press, 2004.

[2] A. Siegman, " Lasers,". University Science Books, 1986.

[3] A. Einstein, "Zur quantentheorie der strahlung," *Physikalische Zeitschrift*, vol. 18, 1917.

[4] H. Eichler, B. Eppich, J. Fischer, R. Güther, G. Gurzadyan, A. Hermerschmidt, A. Laubereau, V. Lopota, O. Mehl, C. Vidal, *et al.*, "Laser physics and applications," *Landolt-Börnstein: Numerical Data and Functional Relationships in Science and Technology*, 2005.

[5] A. L. Schawlow and C. H. Townes, "Infrared and optical masers," *Phys. Rev.*, vol. 112, pp. 1940–1949, Dec 1958.

[6] T. H. Maiman, "Stimulated optical radiation in ruby," *Nature*, vol. 187, pp. 493–494, Aug 1960.

[7] J. F. Ready, " Industrial applications of lasers,". Academic press, 1997.

[8] W. Koechner, " Solid-state Laser Engineering,". Springer series in optical sciences, XII, 1988.

[9] L. Jie, J. Yu-Lei, Y. Ji-Min, D. Juan, and H. Jing-Liang, "Efficient diode-pumped passively Q-switched $Nd{:}GdVO_4$ lasers," *Chinese Physics Letters*, vol. 19, no. 12, pp. 1808–1810, 2002.

[10] X. Zhang, S. Zhao, Q. Wang, Q. Zhang, L. Sun, and S. Zhang, "Optimization of Cr^{4+}-doped saturable-absorber Q-switched lasers," *IEEE Journal of Quantum Electronics*, vol. 33, pp. 2286–2294, Dec 1997.

[11] I. Lăncrănjan, R. Savastru, D. Savastru, and S. Micloş, "Numerical simulation of passively Q-switched solid state lasers,". In Numerical Simulation - From Theory to Industry, pp. 289–308, 2012.

[12] R. C. Botha, " Development of diode end-pumped *Nd:YLF* lasers at 1314 nm for high power operation,". PhD thesis, Stellenbosch University, 2016.

[13] N. Hodgson and H. Weber, " Laser Resonators and Beam Propagation: Fundamentals, Advanced Concepts, Applications,". Springer Series in Optical Sciences, Springer Berlin Heidelberg, 2014.

[14] M. Wohlmuth, C. Pflaum, K. Altmann, M. Paster, and C. Hahn, "Dynamic multimode analysis of Q-switched solid state laser cavities," *Opt. Express*, vol. 17, pp. 17303–17316, Sep 2009.

[15] A. G. Fox and T. Li, "Resonant modes in a maser interferometer," *Bell System Technical Journal*, vol. 40, no. 2, pp. 453–488, 1961.

[16] J. Nelson, " Novel optical resonators,". PhD thesis, University of Glasgow, 2012.

[17] I. Litvin, " Intra-cavity Laser Beam Shaping,". PhD thesis, Stellenbosch University, 2010.

[18] H. Weber, "Collins' integral for misaligned optical elements," *Journal of Modern Optics*, vol. 53, no. 18, pp. 2793–2801, 2006.

[19] J. J. Degnan, "Optimization of passively Q-switched lasers," *IEEE Journal of Quantum Electronics*, vol. 31, pp. 1890–1901, Nov 1995.

[20] L. Niu, C. Gao, S. Zhu, C. Sun, H. He, Z. Song, and W. Tang, "Single- and dual-pulse oscillation in a passively Q-switched *Nd:YAG* microchip laser," *Opt. Express*, vol. 19, pp. 20628–20633, Oct 2011.

[21] D. Naidoo, "Transverse modes in solid-state laser resonators,". Master's dissertation, School of Physics, University of KwaZulu-Natal, 2011.

[22] A. Sennaroglu, "Solid-state lasers and applications," vol. 119, CRC press, 2006.

[23] D. J. Griffiths, " Introduction to quantum mechanics,". Pearson Education India, 2005.

[24] H. Kogelnik and T. Li, "Laser beams and resonators," *Appl. Opt.*, vol. 5, pp. 1550–1567, Oct 1966.

[25] optique-ingenieur, "Geometry of the two-mirrors cavity," *http:www.optique-ingenieur.org/en/courses/OPI_ang_M01_C03/co/Contenu_11.html* [Online; accessed February 01, 2017].

[26] J. Park, C. Cho, C. Lim, K. Ko, D. Kim, H. Cha, and Y. Kang, "Additional laser pulses due to different saturation characteristics of gain and absorption in passively Q-switched lasers," *Conference on Lasers and Electro-Optics/Pacific Rim*, p. WP_022, 2007.

[27] A. Dement'ev, R. Navakas, and R. Vaicekauskas, "Modeling of generation dynamics of passively and actively Q-switched solid-state lasers," *Mathematical modelling and analysis*, vol. 5, no. 1, pp. 32–43, 2000.

[28] G. Xiao and M. Bass, "A generalized model for passively Q-switched lasers including excited state absorption in the saturable absorber," *IEEE Journal of Quantum Electronics*, vol. 33, pp. 41–44, Jan 1997.

[29] J. Zabkar, M. Marincek, and M. Zgonik, "Mode competition during the pulse formation in passively Q-switched *Nd:YAG* lasers," *IEEE Journal of Quantum Electronics*, vol. 44, no. 4, pp. 312–318, 2008.

[30] J. Swiderski, "Optimization of a passively Q-switched *Nd:YAG* laser with a saturable absorber characterized by excited state absorption (esa)," *Optica Applicata*, vol. 34, no. 2, pp. 275–290, 2004.

[31] J. Liu, D. Shen, S.-C. Tam, and Y.-L. Lam, "Modeling pulse shape of Q-switched lasers," *IEEE Journal of Quantum Electronics*, vol. 37, pp. 888–896, Jul 2001.

[32] N. W. Longbotham, "Experimental characterization of Cr^{4+}*:YAG* passively Q-switched *Cr:Nd:GSGG* lasers and comparison with a simple rate equation model,". PhD thesis, The University of New Mexico, 2008.

[33] optique-ingenieur, " Spatial energy distribution for Hermite-Gaussian modes," *http://www.optique-ingenieur.org/en/courses/OPI_ang_M01_C03/co/Contenu_13.html* [Online; accessed February 01, 2017].

[34] S.-C. Chu, Y.-T. Chen, K.-F. Tsai, and K. Otsuka, "Generation of high-order hermite-gaussian modes in end-pumped solid-state lasers for square vortex array laser beam generation," *Optics express*, vol. 20, no. 7, pp. 7128–7141, 2012.

[35] J. Alda, "Laser and gaussian beam propagation and transformation," *Encyclopedia of optical engineering*, vol. 2013, pp. 999–1013, 2003.

[36] W. S. Chang, " Principles of lasers and optics,". Cambridge University Press, 2005.

[37] J. W. Goodman, "Introduction to fourier optics,". Roberts and Company Publishers, 2005.

[38] J. Degnan and D. Hall, "Finite-aperture waveguide-laser resonators," *IEEE Journal of Quantum Electronics*, vol. 9, pp. 901–910, September 1973.

[39] E. H. Bernhanrdi, "Modelling diode-pumped solid state lasers,". Master's dissertation, School of Physics,University of KwaZulu-Natal, 2008.

[40] photonics, "*Nd:YAG* laser line mirrors offer the high reflectance and superior surface quality and accuracy needed for demanding laser applications," *https://www.photonics.com/Article.aspx?AID=61285* [Online; accessed February 01, 2017].

[41] H. Karow, " Fabrication Methods for Precision Optics,". Wiley Series in Pure and Applied Optics, Wiley, 2004.

[42] W. S. Koen, "End pumped solid-state laser,". Master's dissertation, School of Physics,University of KwaZulu-Natal, 2009.

[43] S. Sudheer, S. Prathibha, D. Kothwala, V. M. Pillai, and V. Nayar, "Characterization of an arc lamp pumped, linearly polarized TEM_{00} and Q-switched $Nd{:}YAG$ laser at 1064nm for optical tweezers in interaction force studies in cardio-vascular implant surfaces," *Digest Journal of Nanomaterials & Biostructures (DJNB)*, vol. 4, no. 1, pp. 119–131, 2009.

[44] G. Xiao, J. H. Lim, S. Yang, E. Van Stryland, M. Bass, and L. Weichman, "Z-scan measurement of the ground and excited state absorption cross sections of Cr^{4+} in yttrium aluminum garnet," *IEEE journal of quantum electronics*, vol. 35, no. 7, pp. 1086–1091, 1999.

[45] M. Yin, G. Feng, S. Wang, H. Yang, and S. Zhou, "Spatial and temporal distribution of Q-switched laser pulses in multimode regimes," *Chinese Optics Letters*, vol. 11, no. 12, pp. 121405–121405, 2013.

[46] J. J. Degnan, "Theory of the optimally coupled Q-switched laser," *IEEE Journal of Quantum Electronics*, vol. 25, pp. 214–220, Feb 1989.

[47] S. Forget, F. Druon, F. Balembois, P. Georges, N. Landru, J.-P. Fève, J. Lin, and Z. Weng, "Passively Q-switched diode-pumped $Cr^{4+}{:}YAG/Nd^{3+}{:}GdVO_4$ monolithic microchip laser," *Optics communications*, vol. 259, no. 2, pp. 816–819, 2006.